Dear Author,

Please, note that changes made to the HTML content will be added to the article before publication, but are not reflected in this PDF.

Note also that this file should not be used for submitting corrections.

A complex magmatic system beneath the Kissomlyó monogenetic volcano (western Pannonian Basin): Evidence from mineral textures, zoning and chemistry

M. Éva Jankovics [a,b,*], Szabolcs Harangi [a,c], Károly Németh [d], Balázs Kiss [a,b], Theodoros Ntaflos [e]

[a] MTA-ELTE Volcanology Research Group, Pázmány Péter sétány 1/C, H-1117 Budapest, Hungary
[b] Vulcano Research Group, Department of Mineralogy, Geochemistry and Petrology, University of Szeged, Egyetem utca 2, H-6722 Szeged, Hungary
[c] Department of Petrology and Geochemistry, Eötvös Loránd University, Pázmány Péter sétány 1/C, H-1117 Budapest, Hungary
[d] Volcanic Risk Solutions, Massey University, Private Bag 11 222, Palmerston North, New Zealand
[e] Department of Lithospheric Research, University of Vienna, Althanstrasse 14, A-1090 Vienna, Austria

ABSTRACT

Kissomlyó is a small-volume Pliocene alkaline basaltic eruptive centre located in the monogenetic Little Hungarian Plain Volcanic Field (western Pannonian Basin). It consists of a sequence of pyroclastic and effusive eruptive units: early tuff ring (unit 1), pillow and columnar jointed lava (unit 2), spatter cone (unit 3). The tuff ring sequence is overlain by a unit of lacustrine sediments which suggests a significant time gap in the volcanic activity between the tuff ring formation and the emplacement of the lava flow. High-resolution investigation of mineral textures, zoning and chemistry as well as whole-rock geochemical analyses were performed on stratigraphically controlled samples in order to characterise the magmas represented by the distinct eruptive units and to reveal the evolution of the deep magmatic system.

Based on the bulk rock geochemistry, compositionally similar magmas erupted to the surface during the entire volcanic activity. However, olivine crystals show diverse textures, zoning patterns and compositions reflecting various deep-seated magmatic processes. Five different olivine types occur in the samples. Type 1 olivines represent the phenocryst sensu stricto phases, i.e., crystallised in situ from the host magma. The other olivine types show evidence for textural and compositional disequilibrium reflecting single crystals consisting of distinct portions having different origins. Type 2a and type 2b olivines have antecrystic cores which are derived from two distinct primitive magmas based on the different compositions of their spinel inclusions. Type 4 olivines show reverse zoning whose low-Fo cores represent antecrysts from more evolved magmas. The cores of type 3 and type 5 olivines are xenocrysts originated from the subcontinental lithospheric mantle. These xenocrysts are surrounded by high-Fo or low-Fo growth zones suggesting that olivine xenocryst incorporation occurred at different levels and stages of magma evolution.

Olivine-hosted spinel inclusions show three distinct compositional groups. Group 1 spinels are very Al-rich (0–0.22 Cr#) and coexist with the antecrystic cores of type 2a olivines, group 2 spinels have 44.5–62.3 Cr#s and occur in the phenocryst s.s. (type 1) olivines, while group 3 spinels are very rich in Cr (68.4–81.3 Cr#) and appear in the antecrystic cores of type 2b olivines. Based on the integrated analysis of olivines and their spinel inclusions four magmatic environments were involved into the evolution of the magmatic system. These crystals bear evidence of various petrogenetic processes playing role in the formation of the erupted magma batches: fractional crystallization, olivine (+ spinel) recycling, xenocryst incorporation, magma recharge and interaction of multiple small magma packets in a multi-level magmatic system.

Clinopyroxene-melt thermobarometry yields an average pressure of 6.6 ± 0.9 kbar corresponding to a depth of about 25 km, implying that the main level of final clinopyroxene fractionation could have occurred around the Moho (in the lowermost crust).

This study shows that high-resolution mineral-scale analyses carried out through monogenetic sequences provide a unique, more detailed insight into the evolution of these "simple" magmatic systems as crystal growth stratigraphy and compositions yield direct evidence for various petrogenetic processes which are usually obscured in the whole-rock geochemistry.

© 2015 Published by Elsevier B.V.

* Corresponding author at: Pázmány Péter sétány 1/C, H-1117 Budapest, Hungary. Tel.: +36 1 372 25 00 8359.
E-mail address: m.eva.jankovics@gmail.com (M.É. Jankovics).

1. Introduction

Terrestrial basaltic volcanic fields generally contain numerous small edifices of cinder cones, tuff rings, maars, shield volcanoes and lava flows representing small-volume and short-lived monogenetic eruptive centres. Each of these volcanoes is produced by a single episode of volcanic activity lasting from several days to decades and emitting <1 km³ volumes of magma (e.g., Takada, 1994; Connor and Conway, 2000). On closer inspection, regardless of their small size they often have complex architecture reflecting multiple eruption phases which produced different eruptive units (e.g., Smith et al., 2008; Brenna et al., 2010; Németh, 2010; Sohn et al., 2012). Detailed studies on single volcanic centres revealed significant compositional variations through the sequences and between phases of the eruption that were interpreted as the result of complex melting and mixing processes within the mantle sources, variations in melting conditions or mixing of different magma batches during ascent (e.g., Strong and Wolff, 2003; Brenna et al., 2010, 2011; Erlund et al., 2010; Mcgee et al., 2012; Sohn et al., 2012; Boyce et al., 2015). All of these works rest on whole-rock major and trace element and isotopic compositions, however, less focus has been put on the textures, zoning and chemistry of rock-forming minerals that bear valuable information about the processes acting during the evolution of the magmatic systems (e.g., Streck, 2008). As shown by a number of studies (e.g., Dobosi, 1989; Dobosi et al., 1991; Roeder et al., 2001, 2003, 2006; Reubi et al., 2003; Smith and Leeman, 2005; Jankovics et al., 2009, 2012, 2013; Longpré et al., 2014), the detailed textural and chemical analyses of the phenocryst phases in basaltic rocks can provide unique insights into the details of magma evolution as well as of the mantle source regions.

The Carpathian–Pannonian Region (in Eastern Central Europe) includes several intracontinental monogenetic volcanic fields which are not associated with large-volume composite volcanoes (like for example in the case of Jeju or Etna). They were formed during the Late Miocene–Quaternary alkaline basalt volcanism (e.g., Embey-Isztin et al., 1993; Harangi, 2001a; Harangi and Lenkey, 2007). A number of eruptive centres of these volcanic fields were the subject of extensive research based on physical volcanology and whole-rock geochemistry (e.g., Embey-Isztin et al., 1993; Harangi et al., 1994, 1995; Konečný et al., 1995; Németh et al., 2001; Martin and Németh, 2004, 2005; Seghedi et al., 2004; Auer et al., 2007; Kereszturi et al., 2010; Ali and Ntaflos, 2011), but only a few of them were studied through both detailed mineral-scale investigations and whole-rock chemical analyses (Dobosi, 1989; Jankovics et al., 2009, 2012, 2013; Harangi et al., 2013). Additionally, there are no examples of detailed studies of petrology and geochemistry of the distinct eruptive units through the succession of a given volcanic centre from this region.

This paper focuses on the Kissomlyó eruptive centre, located in the Little Hungarian Plain Volcanic Field (western Pannonian Basin), which shows a complex volcanological architecture consisting of different eruptive units (tuff ring, lava flows, spatter cone). Based on earlier physical volcanological observations a considerable time break was suggested during its volcanic activity (Martin and Németh, 2004, 2005). As the sedimentary evidences of time breaks in monogenetic eruption sequences are potential indications of shifts in eruption chemistry (e.g., Sohn et al., 2012) our aim was to reveal whether there are significant compositional differences between the magmas erupted to the surface before and after the quiescence period. Monogenetic volcanic centres with intermittent activity are only rarely known. The eruptive units of the well-studied Rangitoto volcano (Auckland Volcanic Field, New Zealand) have been produced by two significantly different—an alkaline and a subalkaline—magma batches, it can be characterised by a ~1000 years long intermittent activity and it is much more voluminous than Kissomlyó (Mcgee et al., 2011; Needham et al., 2011; Shane et al., 2013). In addition, there are also some examples for rejuvenating activity in the same locations with a difference of several thousand years (western Saudi Arabian volcanic fields; Németh et al., 2014) or even of millions of years (Hammerunterwiesenthal maar, Saxony; Suhr and

Goth, 2013; although here the 2nd and 3rd phases were only represented by subvolcanic intrusions).

Whole-rock composition represents the composition of the erupted magma which in most cases is the result of several closed- and open-system petrogenetic processes involving discrete magma batches of similar/different compositions. We performed high-resolution textural and chemical investigations of the rock-forming minerals because they respond texturally and compositionally to changing magmatic environments and preserve in their crystal growth stratigraphy a wealth of information concerning the magmatic processes and compositions (e.g., Ginibre et al., 2007; Streck, 2008). This mineral-scale study was integrated with the whole-rock geochemistry of stratigraphically controlled samples deriving from the three eruptive units of Kissomlyó.

2. Geological setting

The Pannonian Basin is a Miocene extensional back-arc basin surrounded by the Alpine, Carpathian, and Dinarides orogenic belts (Fig. 1A). It is characterised by thin lithosphere (50–80 km) and crust (22–30 km) coupled with high heat flow (>80 mW/m²; Csontos et al., 1992; Fodor et al., 1999; Tari et al., 1999; Bada and Horváth, 2001; Lenkey et al., 2002). These features are due to the initial syn-rift phase (17–12 Ma; Horváth, 1995) of the Pannonian Basin that was characterised by subduction roll-back, related back-arc extension and lithospheric thinning (Csontos et al., 1992; Horváth, 1993; Tari et al., 1999). This was followed by the Late Miocene–Pliocene post-rift phase (e.g., Horváth, 1995) which was accompanied by thermal subsidence, thickening of the lithosphere and sedimentation in the basin areas. Tectonic inversion has characterised the Pannonian Basin since the late Pliocene because of the push of the Adriatic plate from the southwest and blocking by the East European platform in the east (Horváth and Cloetingh, 1996).

Post-extensional alkaline basaltic volcanism occurred from 11 to 0.13 Ma in the region, mainly on its marginal parts, which formed monogenetic volcanic fields (Fig. 1A) (e.g., Martin and Németh, 2004; Seghedi et al., 2004; Harangi and Lenkey, 2007). The geodynamic relationships of the alkaline basaltic volcanism are still debated. Several researchers suggested that localised mantle plume fingers (deriving from a common mantle reservoir named "European Asthenospheric Reservoir"; Hoernle et al., 1995) could be responsible for the alkaline basaltic volcanism in Western and Central Europe, accordingly in the Pannonian Basin as well (Granet et al., 1995; Seghedi et al., 2004). However, Harangi and Lenkey (2007), Harangi (2009) and Harangi et al. (2014) **Q4** argued against the plume-related magmatism. They suggest that the significantly stretched Pannonian Basin provided suction in the sublithospheric mantle and generated mantle flow from below the thick lithospheric roots (Alps, North European Platform) which could lead to the partial melting of the heterogeneous upper mantle. The relatively hot asthenospheric material could ascend along the steep lithosphere–asthenosphere boundary.

The Little Hungarian Plain Volcanic Field (Fig. 1B) consists of scattered eroded remnants of tuff rings, maars and scoria cones (e.g., Jugovics, 1968; Harangi et al., 1994, 1995; Martin and Németh, 2004). These volcanic centers are located along strike–slip faults and near to a detachment fault (Rába line) (e.g., Jugovics, 1915, 1916; Tari et al., 1992). The volcanic activity commenced with trachyandesitic to trachytic volcanism (~11–12 Ma) and built up a >1000 m thick volcanic complex (Pásztori, northern part of the volcanic field) that is buried by ~2000 m of Late Miocene to Quaternary sediments (Harangi et al., 1995; Harangi, 2001b). The small basaltic volcanoes in the southern part of the volcanic field were formed during the Early Pliocene based on the earlier K/Ar radiometric age data (~4.5–5.9 Ma; Balogh et al., 1986). The $^{40}Ar/^{39}Ar$ dating carried out in the western part of the Pannonian Basin (Wijbrans et al., 2007) included only the Ság-hegy (5.48 ± 0.01 Ma) and the Kissomlyó (4.63 ± 0.02 Ma) eruptive centres from this region. This volcanic field can be regarded as a tectonically controlled field

Q5 (after Valentine and Hirano, 2007) that is characterised by very low magma flux, small number of eruptive centres and long (even around 1 Myr) quiescence periods between the formation of individual small volcanoes.

3. Volcanological features and eruptive volume

The Kissomlyó eruptive centre is a complex monogenetic volcano that consists of different eruptive units produced by multiple eruption phases (Fig. 1C). First, phreatomagmatic explosions built up a tuff ring (consisting of a ~20 m thick sequence of lapilli tuffs and tuffs) in a terrestrial setting which was followed by the cessation of the volcanism and the deposition of lacustrine sediments (a sequence of siltstone and mudstone) in a crater lake. Later the volcanic activity rejuvenated with lava flow emplacement that resulted in the formation of columnar jointed lava and pillow lava intruding the lacustrine sediments (pillows, pillow breccias, peperite) within the crater. Martin and Németh (2004, 2005) already described the tuff ring pyroclastics, lacustrine sediments and lava flow unit. Based on the presence, features and thickness of the crater lake lacustrine unit they estimated the time gap between the tuff ring formation and the emplacement of the lava flow to be in the order of thousands of years. On the top of the volcanic edifice a spatter cone remnant (Királykő) can be found. The ^{40}Ar/^{39}Ar age of the lava flow unit is 4.63 Ma (Wijbrans et al., 2007). The formation of unit 2 and unit 3 eruptive units can be treated as one main volcanic event after the quiescence period based on their volcanological features.

It would be important to quantify more precisely the time gap between the above-mentioned two eruptive phases therefore we tried to rethink the sedimentary features of the lacustrine unit. As Martin and Németh (2005) have already described, the sedimentary structures of this unit are preserved only in its lower ~70 cm, while its other part is disturbed by lava. In the lower undisturbed ~70 cm it can be observed that the sediment is fine-grained, good sorted and dominantly parallel-laminated indicating suspension settling. It consists of fine (~1 mm thick) alternating dark and light laminae. The exact extent of this siliciclastic unit is difficult to determine, but Martin and Németh (2005) estimated its thickness to be maximum 5 m based on the fact that fluidised sediments occur between the pillows in the entire thickness (~5 m) of the pillow lava. Considering all of these observations they concluded that the lacustrine sedimentation could have taken place over a period of a few thousand years. However, it is notable that there are also some parts of the lacustrine unit characterised by non-uniform, low-angle cross-lamination which imply deposition during water movement (currents) in addition to the predominate suspension settling. This suggests that the laminae cannot be solely interpreted as the products of cyclic sedimentation but a part of them could have been formed through water movement. In addition, it may be more likely that the original thickness of the lacustrine unit should not correspond with the whole thickness of the pillow lava but less sediment could have been enough to get everywhere between the pillows during the intense fluidisation. An additional possibility can be that an extreme weather event (e.g., sudden rainfall, intense wind) might have generated the sedimentation in the crater. These latter three arguments can be
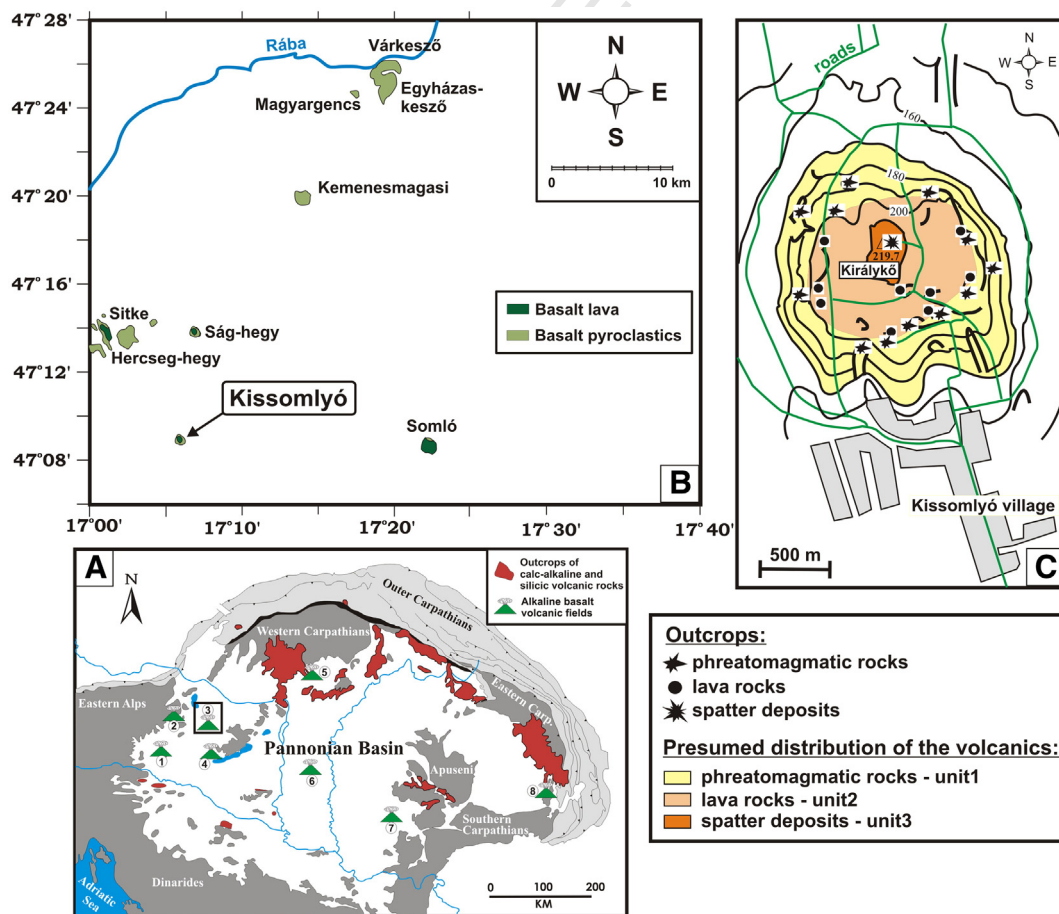
Fig. 1. (A) Geological sketch map of the Carpathian–Pannonian Region. Alkaline basaltic volcanic fields are signed with numbers: 1, Styrian Basin; 2, Burgenland; 3, Little Hungarian Plain, 4, Bakony-Balaton Highland, 5, Štiavnica-Nógrád-Gemer, 6, Kecel, 7, Banat, 8, Perşani. (B) Simplified geological map of the Little Hungarian Plain Volcanic Field (after Jugovics, 1968; Harangi, 2001c) with the names of the volcanic centres. (C) Map of the Kissomlyó volcano showing the outcrops and distribution of the three eruptive units. Contour intervals are 10 m.

241 indicative of a shorter (centuries) time gap between the eruptive
242 phases. Nevertheless, we have to emphasise at this point, that presently
243 there is no unambiguous tool to quantify more precisely the length of
244 this time gap. Therefore, we can conclude now that the quiescence pe-
245 riod in the volcanic activity might have lasted for hundreds to thousands
246 of years.

247 The compound volcanological architecture and the rejuvenation of
248 volcanic activity after a significant pause in the same location imply
249 that this monogenetic volcano could be characterised by a complex
250 evolution and can be regarded as a reactivated eruptive centre.

251 Concerning the eruptive volume of the Kissomlyó volcanics we car-
252 ried out a simple geometric model calculation in absence of a LiDAR or
253 other high-resolution topographic dataset. As the Kissomlyó volcano
254 is an erosional remnant the observed volcanics represent significantly
255 smaller volumes than the original eruptive volumes. The erosion rem-
256 nant morphology was described by Martin and Németh (2005). The
257 tuff ring has a diameter of approximately 800 m and the thickness of
258 its sequence is ~20 m. Considering the effect of the erosion the bulk
259 volume of the tuff ring could have been around 0.01 km^3. The DRE-
260 corrected volume was estimated using 30 vol.% juvenile content and
261 30 vol.% vesicularity following the method of Kereszturi et al. (2013)
262 that resulted in a value of about 0.001 km^3. The bulk volume of the
263 lava unit (having ~400 m diameter and ~20 m thickness) can be esti-
264 mated to around 0.001 km^3. Using 10 vol.% for void space and 15 vol.%
265 vesicularity (also after Kereszturi et al., 2013) the DRE-corrected vol-
266 ume is approximately 0.00064 km^3. The volume of the spatter cone
267 remnant is very small and can be added to the volume of the lava
268 flows which means that the post-tuff ring DRE eruptive volume can
269 be around 0.001 km^3 similarly to that of the tuff ring. Thus, the total
270 DRE volume of the erupted material can be estimated to be maximum
271 0.002 km^3. This value is comparable with those of the smallest volca-
272 nic centres of the Auckland Volcanic Field (Kereszturi et al., 2013)

273 when considering the centres built up by similar eruptive units like
274 Kissomlyó.

4. Samples and analytical methods

276 In this study, we carried out stratigraphically controlled sampling:
277 rock samples that were collected from the three different eruptive
278 units: juvenile basalt fragments (cauliflower bombs) and lapilli
279 tuffs from the tuff ring pyroclastics (unit 1), lava samples from the
280 pillow and columnar jointed basalt (unit 2) and scoria and bomb
281 samples from the spatter deposits (unit 3). During the sampling,
282 our aim was to collect representative samples from each of the dis-
283 tinct eruptive units. The tuff ring sequence does not contain any sed-
284 imentary evidences (e.g., discontinuity/truncation surfaces, erosion
285 contacts, event horizons, etc.) which would imply changes or breaks
286 in the course of the deposition (it is a typical sequence of pyroclastic
287 density currents that could have deposited continuously within
288 hours), therefore a few sample can be considered as representative
289 for unit 1. The poor exposure of unit 2 and unit 3 hindered a more de-
290 tailed sampling.

291 The petrographic investigations were performed with a Nikon
292 YS2-T polarising microscope and an AMRAY 1830 I/T6 scanning elec-
293 tron microscope at the Department of Petrology and Geochemistry of
294 the Eötvös Loránd University (Budapest, Hungary).

295 Whole-rock major and trace element geochemical compositions
296 were analysed at AcmeLabs (Vancouver, Canada; http://acmelab.com/).
297 Major and minor elements were determined by ICP-emission spectrom-
298 etry and trace elements were analysed by ICP-MS following a lithium
299 borate fusion and dilute acid digestion.

300 The in situ analyses of the mineral phases and glasses were per-
301 formed using a CAMECA SX100 electron microprobe equipped with
302 four WDS and one EDS at the University of Vienna, Department of
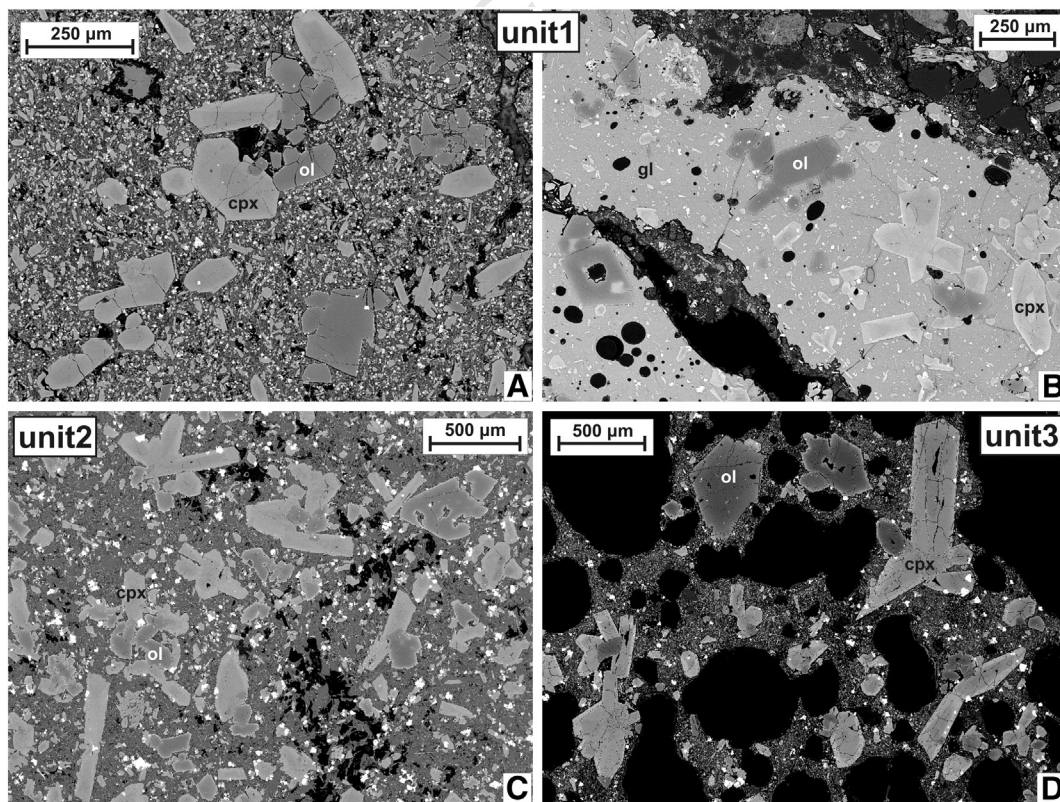
Fig. 2. General textural features of the Kissomlyó basaltic rocks with phenocrysts and microphenocrysts of olivine (with Cr-spinel inclusions), clinopyroxene and minor plagioclase (BSE images): (A) juvenile basalt fragment and (B) sideromelane glass shard from the tuff ring pyroclastics of unit 1; (C) columnar jointed lava sample form unit 2; (D) scoria sample from unit 3. Ol, olivine; cpx, clinopyroxene; gl, glass.

Lithospheric Research (Austria). Operating conditions for minerals were as follows: 15 kV accelerating voltage, 20 nA beam current, 20 s counting time on peak position, focused beam diameter and PAP correction procedure for data reduction. The same operating conditions with 7 μm defocused beam and 10 s counting time were applied for glass analyses. Calibration was based on the following standards: quartz (Si), albite (Na), olivine (Mg), almandine (Al, Fe), wollastonite (Ca), rutile (Ti), spessartine (Mn), orthoclase (K), Mg-chromite (Cr), Ni-oxide (Ni) and apatite (P).

5. Petrography

Each of the studied samples has porphyritic textures with phenocrysts and microphenocrysts of olivine (with spinel inclusions), clinopyroxene (with titanomagnetite inclusions) and minor plagioclase. Compared to the other basaltic rocks of this region, only the Kissomlyó samples contain clinopyroxene as a phenocryst phase. Frequent glomerophyric aggregates of clinopyroxenes, olivines and clinopyroxenes + olivines are also present (Fig. 2). The groundmasses consist of microlitic plagioclase, olivine, clinopyroxene, Fe–Ti-oxides, apatite and glass. Some textural differences can be observed between the samples of the individual eruptive units. The juvenile basalt fragments of unit 1 (Fig. 2A) have medium to highly vesicular textures and are characterised by phenocryst sizes of <0.8 mm where only olivine (<0.8 mm) and clinopyroxene (<0.65 mm) represent the phenocryst and microphenocryst phases, plagioclase occur only in the fine-grained groundmass. The lapilli tuff samples contain abundant fresh sideromelane glass shards (0.15–2 mm in size) which are low to highly vesicular and have the same phenocryst assemblage of olivine and clinopyroxene (Fig. 2B). The textures of the lava rocks of unit 2 (Fig. 2C) have low vesicularity and are coarser-grained compared to the juvenile basalt fragments of unit 1. Phenocrysts have sizes of <1.8 mm (olivine: <0.9 mm, clinopyroxene: <1.8 mm, plagioclase: <0.37 mm), and the groundmass is also coarser-grained and have the highest crystallinity (i.e., contain the smallest amount of glass among the studied samples). The scoria and bomb samples of unit 3 (Fig. 2D) have medium to highly vesicular textures and can be characterised by phenocryst sizes of <1.5 mm (olivine: <0.9 mm, clinopyroxene: <1.5 mm, plagioclase: <0.16 mm) and their groundmass contains a small amount of glass.

Olivine and clinopyroxene often occur together: they are attached to each other or more frequently clinopyroxene surrounds or encloses partly or entirely the olivine (Fig. 2). These features imply that some of the olivines could have crystallised together with the clinopyroxenes, but most of the olivines predated the crystallization of clinopyroxene. In the juvenile basalt fragments of unit 1 there can be also found numerous anhedral quartz xenocrysts (surrounded by tiny clinopyroxenes and glass) and scarce crystal clots of anhedral olivine and orthopyroxene.

6. Whole-rock geochemistry

Earlier bulk rock geochemical data for the Kissomlyó volcanic centre were reported by Embey-Isztin et al. (1993) and Harangi et al. (1994, 1995). For our stratigraphically ordered study samples were analysed from each of the three eruptive units: juvenile basalt fragments from the tuff ring sequence (unit 1), pillow and columnar jointed lava (unit 2) and lava spatter deposits (unit 3). The new bulk rock compositions are given in Table 1 (major element abundances are normalised to 100%, the ratio Fe_2O_3/FeO is set to 0.2 for the calculation of Mg-number). Besides, we have also included and plotted the whole-rock data of Harangi et al. (1995) which represent unit 1 and unit 2 (Fig. 3).

The samples have basanitic, trachybasaltic and basaltic compositions based on their SiO_2 and total alkali contents (Fig. 3A). Compared to the other basaltic rocks in the Little Hungarian Plain Volcanic Field all of the Kissomlyó samples show slightly lower Mg#s (60.4–65.7; $100 * Mg/(Mg + Fe^{2+})$), MgO (6.9–8.7 wt.%) and Cr contents (189–263 ppm) and significantly lower Ni concentrations (84–127 ppm) indicating that they represent more differentiated magmas (as it was also noted by Harangi et al., 1995). Fig. 3B shows that the studied compositions of each eruptive unit of Kissomlyó show very similar chondrite-normalised REE patterns, which are characteristic for basalt compositions in intraplate settings. From unit 2–unit 3 (which compositions almost entirely overlap with each other) to unit 1 the samples show decreasing MgO, Cr and Ni contents as well as almost constant Al_2O_3/CaO ratios and Nd concentrations (Fig. 3C–F).

When comparing the compositional variation from unit 1 to unit 3 (1.8 wt.% MgO, 75 ppm Cr and 44 ppm Ni) with those described through the successions/time of other volcanic centres from other monogenetic fields, it can be observed that the intra-centre chemical variation of Kissomlyó is smaller than each of the others (Fig. 4).

7. Mineral textures, zoning and chemistry

In order to characterise and compare the distinct eruptive units in more detail, careful analyses of mineral textures, zoning and compositions were performed from all of the three units. Compositions of

Table 1
Bulk rock compositions of the studied samples from the three eruptive units.

	Unit 1		Unit 2		Unit 3		
	KS01	KS02	KS03	KS04	KS05	KS06	KS07
SiO_2	46.30	45.75	45.66	45.90	46.29	46.43	45.89
TiO_2	2.37	2.43	2.35	2.40	2.44	2.48	2.44
Al_2O_3	15.38	15.93	15.04	15.56	15.28	15.54	15.77
FeO	7.95	8.24	8.31	8.60	8.42	9.09	8.66
Fe_2O_3	1.59	1.65	1.66	1.72	1.68	1.82	1.73
MnO	0.16	0.15	0.17	0.19	0.17	0.18	0.17
MgO	6.92	7.07	8.32	8.65	8.59	8.73	8.25
CaO	11.55	10.96	9.61	9.63	9.82	9.87	10.05
Na_2O	3.87	3.19	4.43	2.57	2.82	2.22	2.63
K_2O	1.97	2.64	2.56	2.90	2.61	1.78	2.48
P_2O_5	1.04	1.01	0.89	0.91	0.89	0.81	0.92
Mg#	60.80	60.48	64.10	64.19	64.53	63.12	62.93
Ni	84	94	114	113	117	127	115
Cr	203	189	236	254	246	263	250
Co	33.1	34.9	40.0	37.9	40.2	39.5	34.1
Sc	17	19	18	19	19	19	19
V	200	201	212	200	216	218	190
Cs	8.6	0.8	0.7	1.2	1.1	0.7	0.9
Rb	117.3	60.0	60.5	65.5	60.0	32.8	53.9
Ba	931	979	867	856	921	863	1438
Sr	985	1000	958	1020	988	938	1517
La	53.8	52.1	52.3	54.4	53.2	51.6	55.5
Ce	104.8	102.0	104.6	108.2	104.6	101.5	104.7
Pr	11.71	11.53	11.75	12.89	11.76	11.66	12.99
Nd	45.1	45.6	45.2	50.3	47.4	47.5	51.8
Sm	8.05	7.80	8.04	8.76	8.24	8.04	8.67
Eu	2.35	2.31	2.40	2.56	2.45	2.46	2.59
Gd	6.87	6.89	6.96	7.03	6.95	6.90	7.25
Tb	0.97	0.94	0.96	0.84	0.97	0.97	0.87
Dy	4.81	4.79	4.82	5.18	4.70	4.77	5.11
Ho	0.84	0.84	0.84	0.85	0.82	0.84	0.87
Er	2.05	2.02	2.13	2.22	2.11	1.98	2.19
Tm	0.30	0.29	0.29	0.32	0.29	0.29	0.30
Yb	1.74	1.73	1.74	1.78	1.74	1.73	1.81
Lu	0.27	0.25	0.25	0.26	0.25	0.24	0.26
Hf	6.60	6.80	6.30	7.40	6.50	6.80	7.50
Nb	76.7	75.7	78.3	84.5	79.9	77.3	83.5
Ta	4.70	4.50	4.90	4.80	4.90	4.60	5.40
Th	9.30	9.10	8.50	8.50	8.90	8.40	9.20
U	2.20	2.30	2.80	2.40	2.40	1.70	2.60
Pb	12.1	14.5	29.9	7.5	9.3	10.4	7.6
Zr	279	277	278	295	285	279	284
Y	23.8	22.9	23.0	26.2	23.8	23.7	26.3

Major elements are in wt.%; minor and trace elements are in ppm. Analyses are recalculated to 100% loss free.
Mg# = $100*Mg/(Mg + Fe^{2+})$, where Mg and Fe^{2+} are cation fractions; Fe^{2+} is calculated assuming Fe2O3/FeO = 0.2.

Fig. 3. Whole-rock compositions of the Kissomlyó samples from the three eruptive units: (A) TAS diagram (after LeBas et al., 1986); (B) chondrite-normalised (Nakamura, 1974) REE variation diagram; (C) MgO (wt.%) vs. Al$_2$O$_3$/CaO plot; (D) MgO (wt.%) vs. Cr (ppm) diagram; (E) Cr (ppm) vs. Ni (ppm); (F) Nd (ppm) vs. Ni (ppm) plot. Glass compositions measured from the sideromelane shards (unit 1) and groundmass glass (unit 3) are also plotted in (A) and (C). The ol, ol + cpx, cpx, Cr-sp arrows are indicative of trends of olivine, olivine + clinopyroxene, clinopyroxene, Cr-spinel fractionation, respectively. Frac.cryst. arrow represents a fractional crystallization trend. In the case of two samples, Ni was not analysed.

olivine, spinel and clinopyroxene crystals (Fig. 5) as well as glasses were analysed from juvenile basalt fragments and fresh sideromelane glass shards of unit 1, from lava samples of unit 2 and from scoria and bomb samples of unit 3.

7.1. Olivine

Olivine crystals of the studied rocks show variable textures, zoning patterns and compositions; five different types can be distinguished: type 1, type 2, type 3, type 4 and type 5 olivines (Fig. 6). Type 1 olivines (Fig. 6A) are normally zoned, euhedral-subhedral, often skeletal with Fo$_{81–86}$ cores and Fo$_{75–85}$ rims. From their cores to rims, they have increasing CaO (from 0.16–0.36 wt.% to 0.23–0.46 wt.%) and decreasing NiO contents (from 0.12–0.31 wt.% to 0.08–0.22 wt.%). Type 2 olivines (Fig. 6B) are normally zoned, euhedral to subhedral, and they have subhedral–anhedral Fo$_{86–95}$ cores and often skeletal Fo$_{80–85}$ rims. Their cores contain 0.10–0.62 wt.% CaO and 0–0.41 wt.% NiO, while their rims have 0.25–0.48 wt.% CaO and 0.09–0.21 wt.% NiO contents. The type 2 olivine crystals can be divided into two subtypes—type 2a and type 2b—based on the chemistry of the spinel inclusions in the cores of the host olivines: the cores of type 2a olivines contain Al-rich spinels, while those of type 2b olivines have Cr-rich spinels (Fig. 8B, D). Type 3 olivines (Fig. 6C) have normal zoning; they are euhedral to anhedral and contain 89–91 mol% Fo in their anhedral cores (often with irregular shapes) and 79–85 mol% Fo in their often skeletal rims. The cores have 0.02–0.05 wt.% CaO and 0.34–0.45 wt.% NiO concentrations, whereas the rims contain 0.28–0.31 wt.% CaO and 0.11–0.23 wt.% NiO. Type 4 olivines (Fig. 6D, E) are reversely zoned, euhedral to subhedral; they have subhedral–anhedral (rarely patchy) cores and their rims are frequently skeletal. Their cores have Fo contents varying between 66 and 85 mol%, which are either surrounded by only a (10–40 μm thick) Mg-richer rim of 82–84 mol% Fo or by a normally zoned rim Fo$_{76–86}$ (i.e., a 20–60 μm
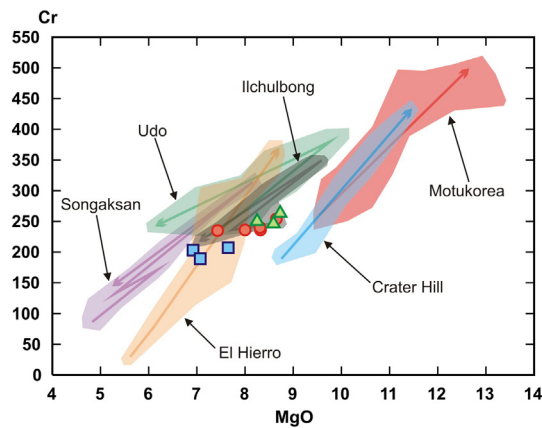
Fig. 4. MgO (wt.%) vs. Cr (ppm) plot showing the chemical variations through time/successions also in the case of other monogenetic volcanoes: Crater Hill (Smith et al., 2008) and Motukorea (Mcgee et al., 2012), Auckland Volcanic Field; Udo (Brenna et al., 2010), Songaksan (Brenna et al., 2011) and Ilchulbong (Sohn et al., 2012), Jeju Island Volcanic Field; El Hierro, 2011–2012 activity, Canary Islands (Martí et al., 2013). Symbols for the Kissomlyó data as in Fig. 3.

thick growth band of Fo_{80-86} and a 10–40 μm final rim Fo_{76-84}). They contain 0.10–0.31 wt.% CaO and 0.02–0.27 wt.% NiO in the cores, and 0.22–0.39 wt.% CaO and 0.08–0.27 wt.% NiO in the rims. Type 5 olivines (Fig. 6F) are multiple-zoned; they have an anhedral rounded core of Fo_{89-90}, 0.02–0.03 wt.% CaO and 0.36–0.38 wt.% NiO (with rare orthopyroxene inclusions) that is surrounded by a growth zone of Fo_{83-85}, 0.22–0.24 wt.% CaO, 0.18–0.22 wt.% NiO and a normally zoned skeletal rim of Fo_{82-86}, 0.22–0.38 wt.% CaO and 0.10–0.25 wt.% NiO. Fig. 7 shows the different core-to-rim compositional variations observed within type 1, type 2, type 3, type 4 and type 5 olivine crystals. Representative olivine compositions are given in Table 2.

Olivine crystals of the five different types occur in the samples of each eruptive unit. Type 1 olivines are the most common ones in each sample. The sideromelane glass shards of unit 1 contain only type 1 olivines. Type 2, type 3 and type 5 olivines occur with very similar frequencies in the three eruptive units, however, type 4 crystals are much more frequent in the juvenile basalt fragments of unit 1 (their amount is twice as much as in the unit 2–unit 3 samples). Type 2a olivines are present in the samples of unit 2 and unit 3, and type 2b olivines were found in those of unit 1 and unit 2. Unit 1 samples can be characterised by the broadest range of olivine Fo contents (66–91 mol%) caused by the variety of the cores of the type 4 (reversely zoned) crystals that is much more limited in unit 2 and unit 3.

7.2. Spinel

Spinels occur as inclusions in several portions of each olivine type: in all parts of type 1 olivines, in the cores and rims of type 2a and type 2b olivines, and in the rims of type 3, type 4 and type 5 crystals (Figs. 6 and 8). The cores of type 3, type 4 and type 5 olivines do not contain any spinel inclusions in the studied samples. The sizes of the spinels range from 2 to 20 μm; they are euhedral to subhedral crystals and have a homogeneous interior. Based on their locations and characteristics, three spinel groups can be distinguished. Group 1 spinels (occurring in unit 2 and unit 3 samples) have a light green colour; they are very Al-rich (57.3–63.1 wt.% Al_2O_3 and 0–0.21 wt.% Cr_2O_3); their Cr#s ($100 * Cr/(Cr + Al)$) are very low (0–0.22) and contain 0.03–3.3 wt.% TiO_2 (Fig. 8C). They occur only in the cores of type 2a olivines (Figs. 6B and 8D). Group 2 spinels (occurring in the samples of each unit) represent the dominant spinel group; they are light brown, have 10.9–23 wt.% Al_2O_3 and 14.8–34.3 wt.% Cr_2O_3 concentrations; their Cr# varies from 44.5–62.3 and show variable TiO_2 contents (1.9–7.2 wt.%) (Fig. 8C). They are present in all portions of type 1 olivines (Figs. 6A and 8A), in the rims of type
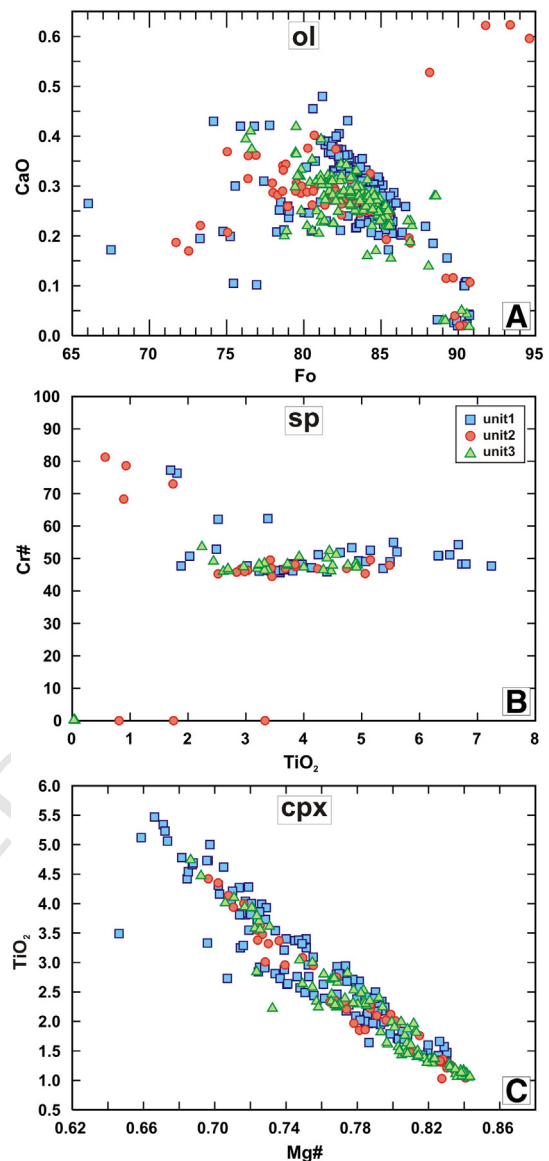
Fig. 5. Mineral compositions of the Kissomlyó samples from the three eruptive units: (A) olivine Fo (mol%) vs. CaO (wt.%) plot; (B) spinel TiO_2 (wt.%) vs. Cr# ($100 * Cr/(Cr + Al)$) diagram; (C) clinopyroxene Mg# ($Mg/(Mg + Fe^{tot})$) vs. TiO_2 (wt.%) variation.

2a and type 2b olivines (Fig. 8B, D), as well as in the rims of type 3 (Fig. 6C), type 4 (Figs. 6D and 8E) and type 5 (Fig. 6F) crystals. Group 3 spinels (occurring in unit 1 and unit 2 samples) are dark brown to black; they are very rich in Cr (41.4–51.1 wt.% Cr_2O_3 and 7.9–12.9 wt.% Al_2O_3); their Cr#s are the highest (68.4–81.3) and contain 0.57–1.8 wt.% TiO_2 (Fig. 8C). They occur only in the cores of type 2b olivines (Fig. 8B). It is important to note that in the case of type 2a and type 2b olivine crystals spinels of the distinct compositional groups were found to be inclusions within the same olivine crystals (Fig. 8B, D). Representative spinel compositions are presented in Table 3.

7.3. Clinopyroxene

Clinopyroxene phenocrysts are euhedral to subhedral and most often appear as glomerocrysts. They frequently contain olivine crystals as inclusions (Fig. 9A) or partly enclose them (Fig. 9B). Characteristically they show sector zoning that displays highly variable appearances and usually, oscillatory zoning is associated with hour-glass zoning (Fig. 9A, B).
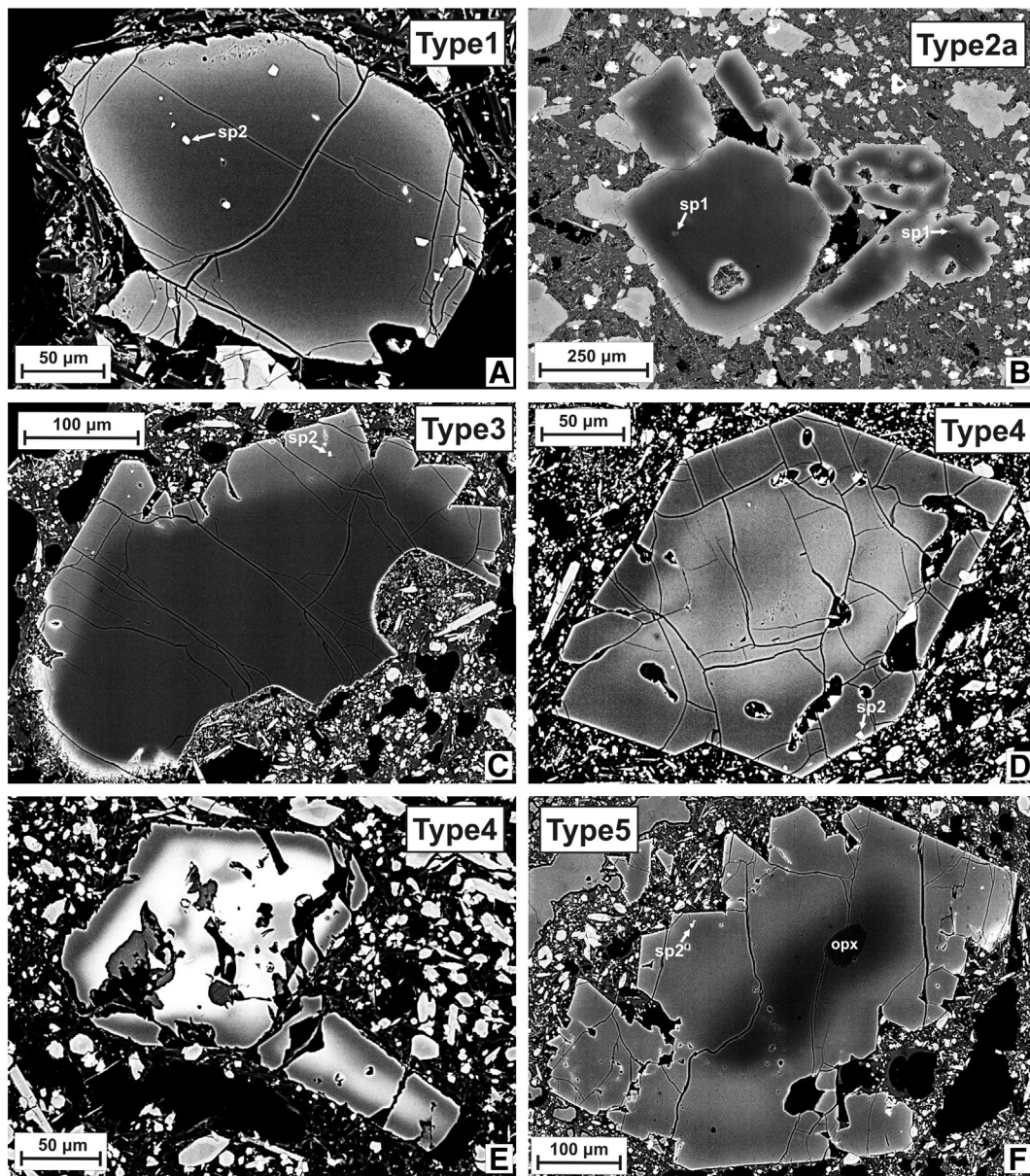
Fig. 6. Textural and zoning characteristics of the studied olivine crystals (BSE images): (A) subhedral type 1 olivine with normal zoning; (B) clot of subhedral type 2a olivine crystals with normal zoning; (C) type 3 olivine with an anhedral core, a subhedral–euhedral rim and normal zoning (note the irregular shape of the core which is only partly surrounded by the rim); (D) euhedral type 4 olivine with reverse zoning, a subhedral core and a skeletal rim; (E) euhedral type 4 olivine showing reverse zoning and a subhedral, patchy core; (F) type 5 olivine characterised by multiple zoning: an anhedral high-Fo core (with an orthopyroxene inclusion), a growth zone with lower Fo and a normally zoned skeletal rim. All types of olivines contain spinel inclusions in some of their portions: sp1 and sp2 refers to group 1 and group 2 spinels, respectively seen in Fig. 8. Sp, spinel; opx, orthopyroxene.
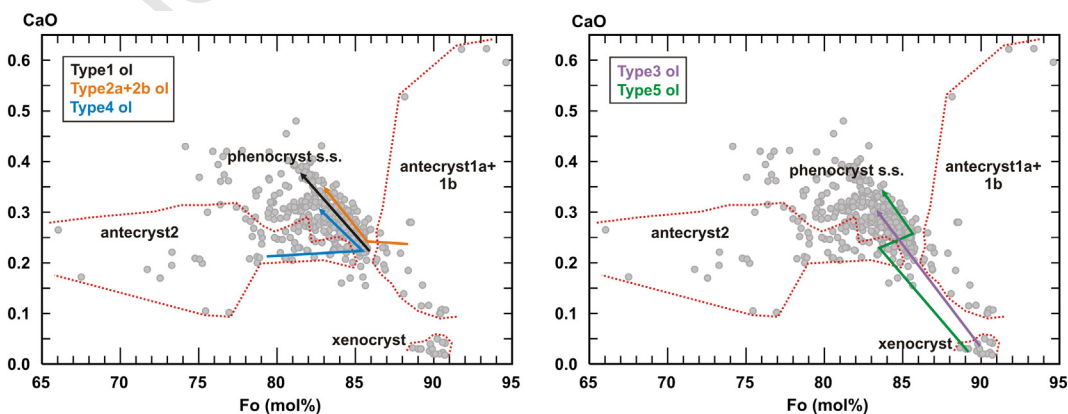
Fig. 7. Forsterite (mol%) vs. CaO (wt.%) plot of the studied olivines. The arrows of different colours indicate the observed intra-crystal core-to-rim compositional variations in the case of the five different olivine types. Antecryst 1a + 1b, antecryst 2, xenocryst and phenocryst *s.s.* refer to the distinct origins of olivines (see text for explanation).

ARTICLE IN PRESS

Table 2
Representative compositions of the studied olivine crystals.

	Type 1 olivine								Type 2 olivine								Type 3 olivine		
	Core	Rim	Core	Rim	Core	Rim	Core	Rim	Core	Rim	Core	Rim	Core	Rim	Core	Rim	Core	Rim	Core
	ol1_1	ol1_2	ol2_1	ol2_2	ol3_1	ol3_2	ol4_1	ol4_2	ol5_1	ol5_2	ol6_1	ol6_2	ol7_1	ol7_2	ol8_1	ol8_2	ol9_1	ol9_2	ol10_1
SiO_2	39.98	39.32	39.86	39.02	39.31	38.97	40.96	39.54	40.92	39.50	40.38	40.00	40.49	39.64	41.19	39.67	41.16	40.06	40.92
MgO	45.18	43.56	44.54	41.28	43.11	39.82	48.43	43.62	47.55	42.42	46.42	44.54	47.63	44.00	48.69	43.08	49.40	45.50	48.54
FeO^{tot}	13.88	15.49	15.01	18.58	16.36	20.02	9.94	15.94	11.06	16.99	12.50	14.28	11.17	15.62	9.41	16.44	9.17	14.20	9.51
CaO	0.21	0.30	0.26	0.33	0.24	0.29	0.12	0.31	0.28	0.29	0.19	0.27	0.19	0.31	0.05	0.31	0.02	0.28	0.02
NiO	0.26	0.13	0.24	0.12	0.16	0.10	0.30	0.17	0.11	0.16	0.19	0.20	0.35	0.16	0.39	0.16	0.41	0.23	0.38
MnO	0.27	0.31	0.28	0.37	0.29	0.42	0.14	0.27	0.19	0.29	0.24	0.27	0.17	0.28	0.14	0.30	0.16	0.26	0.13
Total	99.93	99.17	100.27	99.83	99.64	99.71	99.97	99.95	100.21	99.75	99.98	99.63	100.07	100.06	99.88	100.04	100.35	100.60	99.52
Fo (mol%)	85.29	83.36	84.10	79.83	82.45	78.00	89.67	82.99	88.46	81.66	86.88	84.76	88.37	83.39	90.22	82.36	90.57	85.10	90.10

FeO^{tot} = total amount of iron; ol = olivine.

Table 2 (*continued*)

	Type 3 olivine					Type 4 olivine						Type 5 olivine							
	Rim	Core	Rim	Core	Rim	Core	Normally zoned rim		Core	Normally zoned rim		Core	Growth zone	Normally zoned rim		Core	Growth zone	Normally zoned rim	
	ol10_2	ol11_1	ol11_2	ol12_1	ol12_2	ol13_1	ol13_2	ol13_3	ol14_1	ol14_2	ol14_3	ol15_1	ol15_2	ol15_3	ol15_4	ol16_1	ol16_2	ol16_3	ol16_4
SiO_2	39.59	37.10	39.17	39.55	39.83	38.81	39.82	39.30	37.35	38.87	38.04	40.94	39.65	40.00	39.77	41.11	40.15	40.20	39.78
MgO	42.75	33.34	42.60	44.01	45.31	41.66	44.53	41.98	36.07	42.13	38.87	48.39	43.15	44.79	43.92	47.75	44.30	44.99	42.87
FeO^{tot}	16.68	28.59	17.12	15.66	13.92	18.17	14.92	17.85	24.33	17.07	21.40	9.62	15.91	13.78	15.18	10.35	14.57	13.56	15.63
CaO	0.29	0.17	0.37	0.22	0.25	0.25	0.29	0.35	0.17	0.31	0.36	0.02	0.24	0.26	0.31	0.03	0.22	0.22	0.29
NiO	0.16	0.04	0.13	0.20	0.21	0.14	0.21	0.10	0.14	0.15	0.08	0.38	0.18	0.21	0.18	0.36	0.20	0.25	0.13
MnO	0.29	0.40	0.35	0.28	0.23	0.30	0.27	0.36	0.49	0.33	0.51	0.14	0.28	0.26	0.27	0.15	0.23	0.24	0.32
Total	99.87	99.78	99.74	100.01	99.83	99.40	100.12	100.06	98.66	99.01	99.39	99.52	99.53	99.42	99.72	99.76	99.78	99.56	99.13
Fo (mol%)	82.04	67.51	81.60	83.36	85.30	80.34	84.17	80.74	72.54	81.47	76.40	89.97	82.86	85.28	83.76	89.16	84.42	85.54	83.02
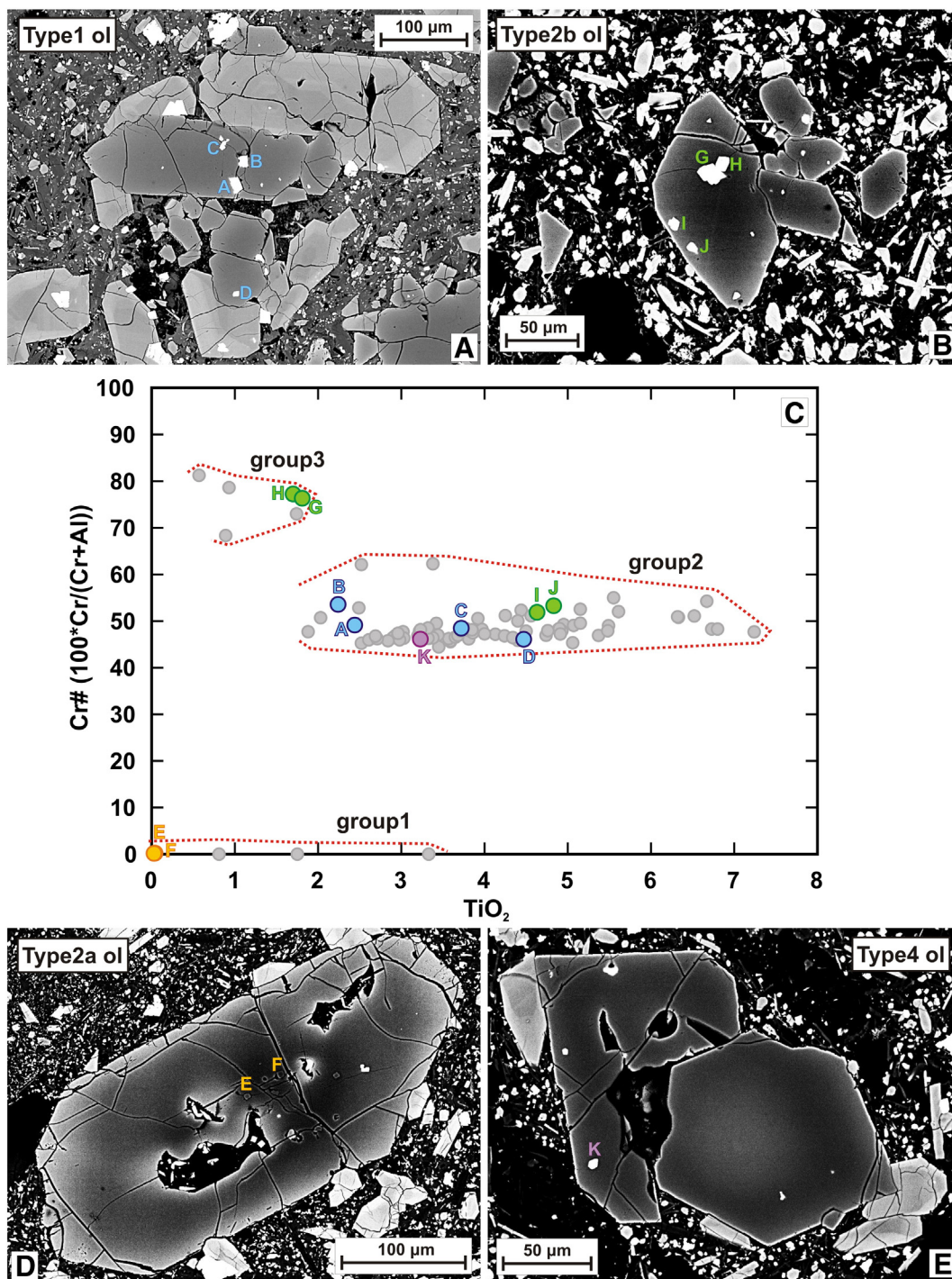
Fig. 8. Textural control of the distribution of olivine-hosted spinel inclusions and their compositional variation. Spinels occur (A) in various portions of type 1 olivines, in the cores and rims of (B) type 2b and (D) type 2a olivines, (E) in the growth zones/rims of type 4 olivines. (C) Plot of TiO₂ (wt.%) vs. Cr# ($100 * Cr/(Cr + Al)$) that shows three distinct compositional groups of the studied spinels. The coloured points with letters indicate the compositions of spinels which are marked with coloured letters in the BSE images.

Table 4 contains representative compositions of the studied clinopyroxenes; they are ferroan diopsides (according to the I.M.A. classification of pyroxenes; Morimoto et al., 1988). Their Mg#s ($Mg/(Mg + Fe^{tot})$) ranges from 0.65 to 0.84 which decrease with increasing TiO₂ (1–5.5 wt.%) and decreasing Cr₂O₃ (0–0.97 wt.%) contents. These compositional variations follow the normal pyroxene fractionation trend (e.g., Tracy and Robinson, 1977). In addition, the observed trends reflect their sector zoning feature: the two trends represent the compositional variation of the Ti-rich and Ti-poor sectors

(Fig. 5C) (Dobosi et al., 1991). The clinopyroxene compositions and trends of the three eruptive units are very similar (Fig. 5C).

7.4. Glass

Glass compositions were measured from the fresh sideromelane glass shards of the lapilli tuff samples of unit 1 and from groundmass glasses of the scoria and bomb samples of unit 3 (Table 5). The glass in the sideromelane shards (unit 1) are fairly homogeneous and have

Table 3

Representative analyses of the studied spinel inclusions in olivines.

	Group 1 sp			Group 2 sp			Group 3 sp		
	sp1	sp2	sp3	sp4	sp5	sp6	sp7	sp8	sp9
SiO_2	0.68	0.13	1.28	0.08	0.08	0.09	0.09	0.07	0.07
TiO_2	1.75	0.04	0.05	2.61	4.13	5.61	1.81	0.57	0.93
Al_2O_3	60.71	63.11	61.09	21.59	17.28	12.95	9.64	7.91	8.86
Cr_2O_3	0.01	0.21	0.02	27.38	22.99	20.95	46.29	51.14	48.59
Fe_2O_3	5.45	5.27	6.12	15.95	20.44	24.72	10.62	7.84	10.15
FeO	5.74	9.18	9.15	18.98	20.65	23.34	18.54	23.53	21.19
MnO	0.08	0.11	0.12	0.27	0.30	0.35	0.25	0.45	0.30
MgO	24.78	21.26	22.18	11.64	10.47	9.25	10.07	5.86	7.88
NiO	0.00	0.12	0.13	0.18	0.18	0.17	0.12	0.02	0.09
Total	99.19	99.44	100.14	98.83	96.57	97.62	97.47	97.39	98.06
Mg#	0.88	0.80	0.81	0.52	0.47	0.41	0.49	0.31	0.40
Cr#	0.01	0.22	0.02	45.96	47.16	52.03	76.32	81.26	78.63

Fe_2O_3 is calculated on the basis of stoichiometry; $Mg\# = Mg/(Mg + Fe^{2+})$; $Cr\# = 100*Cr/(Cr + Al)$; sp = spinel.

phonotephritic compositions (Fig. 3A) with 3.1–3.3 wt.% MgO, while the groundmass glasses (unit 3) have more variable and more evolved tephriphonolitic compositions (Fig. 3A) with 1.1–2.3 wt.% MgO.

8. Thermobarometry

Mineral-melt thermobarometric calculations were performed to estimate the pressures and temperatures of clinopyroxene crystallization. We applied the clinopyroxene-melt geothermobarometer of Putirka et al. (2003) which is based on the jadeite–diopside/hedenbergite–liquid and jadeite–liquid exchange equilibrium. The standard error of estimate of this calibration is 1.7 kbar and 33 °C. For the calculations we used the compositions of clinopyroxene rims and glasses, i.e., we estimated the conditions of the last equilibration. All of the studied clinopyroxene crystals show sector zoning which is a common feature of clinopyroxenes in basaltic rocks. As the two sectors grow contemporaneously from the same liquid (e.g., Wass, 1973), the appropriate way for using these crystals for the calculations is to measure their rim compositions in both sectors and average these values for each crystal.

Pressure and temperature values were calculated for all of the three studied eruptive units which contain the same clinopyroxene population, i.e., their clinopyroxene rim compositions are very similar. In order to test whether the melt compositions are in equilibrium with the clinopyroxene rim compositions, first the observed and predicted values of clinopyroxene components (DiHd, EnFs, CaTs) were compared. Predicted components were obtained by the clinopyroxene saturation model of Putirka (1999) which should be matched by the measured components within the $\pm 2\sigma$ level. Additionally, we tested

the Fe–Mg exchange equilibrium between clinopyroxene and melt: $K_D(Fe–Mg)$ are expected to be 0.28 ± 0.08 (Putirka, 2008). For unit 1 we used the average glass composition of the sideromelane glass shards (which show a restricted range of compositions) from the lapilli tuff samples; for unit 2 there are not any available glass compositions because of the high crystallinity of the groundmass of the lava samples; for unit 3 we used the compositions of the groundmass glasses. Clinopyroxene–liquid pairs of unit 1 are in equilibrium with each other; however, those of unit 3 failed the equilibrium tests because the compositions of the groundmass glasses are too evolved to be in equilibrium with the clinopyroxene rims.

Fig. 3C shows that the glass compositions of the sideromelane shards can be derived from the whole-rock compositions through olivine + clinopyroxene crystallization, and the more evolved groundmass glass compositions can be the result of additional clinopyroxene crystallization. This suggests that in the case of unit 2–unit 3 the average glass composition of the sideromelane shards from unit 1 can be also used as an appropriate liquid composition that is in equilibrium with all of the measured clinopyroxene rim compositions of each unit.

For all of the three units the thermobarometric calculations yield pressures ranging from 5.2 to 8.5 kbar with an average of 6.6 ± 0.9 kbar. Calculated crystallization temperatures range between 1058 and 1089 °C (with an average of 1071 ± 8 °C).

9. Discussion

9.1. Sources for the diverse olivine and spinel populations

Olivine crystals of the studied samples from the three eruptive units show a large diversity of textures, zoning patterns and compositions (Figs. 5–7) reflecting a complex evolution history of the deep magmatic system in which both open- and closed-system processes operated. Fig. 10 summarises the characteristics of the different olivine types together with our interpretations concerning their origin and history.

Type 1 olivine crystals (Fig. 10A) being the most frequent olivine type in each eruptive unit and based on their textures and chemistry (Figs. 6A and 7), represent the olivine phenocryst *s.s.* (phenocryst *sensu stricto*) phases, i.e., the olivines which grew in situ from the host magma. However, the observed core-to-rim zoning in the case of the other olivine types (Figs. 7 and 10B–F) must have been caused by perturbations in intensive variables over their history. Since the Fe^{2+}/Mg ratio of the liquid has the dominant control on the Fo content (Roeder and Emslie, 1970), significant steps in Fo within a given olivine crystal must be due to changes in the composition or oxidation state of the liquid. In the case of the type 2, type 3, type 4 and type 5 olivines the observed zoning in Fo is accompanied by variations in Ca and Ni, which are insensitive to fO_2. Thus, we conclude that these zoning characteristics
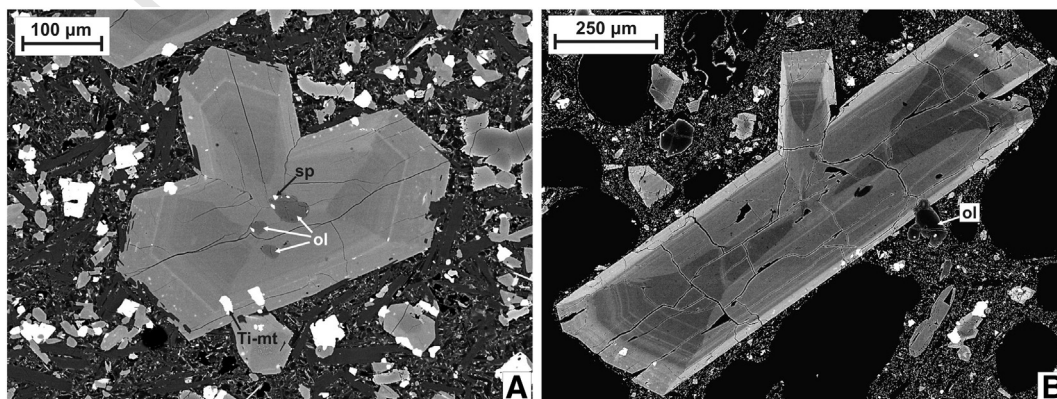
Fig. 9. General features of clinopyroxene phenocrysts: sector zoning and associated concentric zones. (A) Clinopyroxene containing olivine grains (with spinels) as inclusions in the core as well as Ti-magnetite inclusions in the rim; (B) large clinopyroxene phenocryst and a partly enclosed small olivine in its rim. Ol, olivine; sp, spinel; Ti-mt, titanomagnetite.

Table 4
Representative compositions of the studied clinopyroxenes.

| | cpx1 | | | | cpx2 | | | | cpx3 | | | |
| | Sector 1 | | Sector 2 | | Sector 1 | | Sector 2 | | Sector 1 | | Sector 2 | |
	Core	Rim	Core	Rim	Core	Rim	Core	Rim	Core	Rim	Core	Rim
SiO_2	49.94	44.31	46.51	41.99	50.53	47.48	47.32	43.13	50.86	47.14	47.21	43.08
TiO_2	1.35	3.29	2.41	4.78	1.18	2.37	2.12	4.00	1.05	2.29	1.99	4.10
Al_2O_3	3.75	8.73	6.98	10.25	3.62	5.40	6.65	9.22	3.47	5.80	6.72	9.54
Cr_2O_3	0.30	0.00	0.48	0.01	0.43	0.00	0.60	0.02	0.57	0.00	0.95	0.00
Fe_2O_3	2.82	4.71	3.49	4.46	2.36	3.26	3.34	5.71	1.61	3.73	3.08	4.85
FeO	3.17	3.83	3.14	4.60	3.22	4.16	2.94	2.70	3.66	3.56	2.99	3.63
MnO	0.16	0.11	0.09	0.13	0.11	0.17	0.11	0.14	0.14	0.15	0.10	0.11
MgO	14.77	11.42	12.93	10.34	15.11	13.12	13.23	11.10	15.33	12.99	13.31	11.03
CaO	23.00	22.58	22.65	22.28	22.63	23.08	22.74	23.07	22.40	23.24	22.35	22.88
Na_2O	0.38	0.58	0.53	0.61	0.48	0.35	0.59	0.64	0.41	0.38	0.60	0.54
Total	99.68	99.58	99.25	99.44	99.69	99.39	99.63	99.77	99.51	99.31	99.30	99.76
Mg#	0.82	0.72	0.79	0.68	0.83	0.77	0.80	0.72	0.84	0.77	0.80	0.71
En	42.69	35.42	39.43	33.07	43.87	38.84	40.13	34.53	44.60	38.59	40.75	34.44
Wo	47.79	50.33	49.67	51.23	47.24	49.10	49.58	51.56	46.83	49.63	49.18	51.36
Fs	9.51	14.25	10.90	15.70	8.88	12.06	10.29	13.91	8.57	11.79	10.08	14.20

Fe2O3 is calculated on the basis of stoichiometry; Mg# = Mg/(Mg + Fe^{tot}); cpx = clinopyroxene.

are the result of open-system processes involving multiple melts of different compositions.

Type 2 olivines (Figs. 6B and 10B, C) contain a resorbed high-Mg core whose xenocrystic origin can be ruled out due to their higher CaO (0.10–0.62 wt.%) and variable NiO (0–0.41 wt.%) contents. In addition, the shapes, sizes and compositions of the spinel inclusions encapsulated in these cores clearly infer that these olivines have magmatic origin. Consequently, they can be regarded as antecrysts, i.e., cognate crystals that originate from a magma genetically related to the one in which they are found. These antecrysts are surrounded by rims of phenocryst s.s. origin.

The anhedral, resorbed high-Fo, low-CaO, high-NiO cores of type 3 and type 5 olivines (Figs. 6C, F and 10D, F) have compositions characteristic for olivines found in lithospheric mantle-derived peridotites (e.g., Boudier, 1991; Hirano et al., 2004). Thus, they represent olivine xenocrysts derived from the wall rock in the lithospheric mantle which are overgrown by magmatic olivine (as described also in the case of other eruptive centres from the western Pannonian Basin; Jankovics et al., 2013). Occasionally, these olivine cores contain orthopyroxene (enstatite) inclusions (Fig. 6F) and in some cases orthopyroxene (enstatite) crystals are also attached to anhedral olivines having compositions very similar to those of the magnesian cores of type 3 and type 5 olivines. As these orthopyroxenes show compositions (e.g., Mg#(Fe^{tot}) = 0.91) characteristic for mantle-derived peridotites (e.g., Embey-Isztin et al., 2001), this observation also support the lithospheric mantle origin for the cores of the type 3 and type 5 olivines. In the case of type 3 crystals the skeletal overgrowth rim is only of

Table 5
Representative analyses of the studied glasses (normalised to 100% on a volatile-free basis).

| | Sideromelane glass shard | | | Groundmass glass | | |
	gl1	gl2	gl3	gl4	gl5	gl6
SiO_2	48.15	47.50	48.38	49.79	51.69	50.85
TiO_2	2.45	2.39	2.35	2.18	2.01	1.91
Al_2O_3	19.03	19.09	19.32	20.47	22.06	21.54
FeO^{tot}	8.75	8.59	8.81	8.67	6.50	7.22
MgO	3.32	3.19	2.98	2.34	1.27	1.60
MnO	0.18	0.19	0.19	0.15	0.17	0.15
CaO	8.20	8.31	7.41	4.15	4.65	5.06
Na_2O	4.89	5.81	5.55	4.99	3.27	4.19
K_2O	3.58	3.57	3.76	5.95	7.27	6.35
P_2O_5	1.27	1.17	1.10	1.14	0.88	0.94
Mg#	40.32	39.85	37.58	32.46	25.84	28.37

FeO^{tot} = total amount of iron; Mg# = molar MgO/(MgO + FeOtot); gl = glass.

phenocryst s.s. origin, however, the cores of type 5 olivines are surrounded by a rounded lower-Fo growth zone followed by the phenocrystic (s.s.) final rim. This latter feature indicate that the xenocrystic cores of type 5 olivines were incorporated by a more evolved (compared to the host) magma and then a final rim crystallised from the host magma (phenocryst s.s.).

The reverse zoning itself indicates open-system processes (Streck, 2008) in the case of type 4 olivines (Figs. 6D–E and 10E). The resorbed cores of these olivines can be characterised by variable Fo contents (66–85 mol%) and represent antecrysts (antecryst2; Fig. 7) deriving from a magma other than the host. The often normally zoned rims surrounding these cores have phenocryst s.s. origin. Cores of reversely zoned olivines can represent crystals which were formed through magma differentiation in a magma reservoir/storage zone. The more magnesian growth bands and rims (i.e., the normally zoned rims) surrounding these cores can be attributed to the arrival of more primitive magma into the more evolved reservoir (replenishment) followed by crystal fractionation (e.g., Kahl et al., 2011; Martí et al., 2013).

The diverse olivine populations are accompanied by the variety of spinel inclusions. Group 2 spinels representing the dominant spinel group can be regarded as phenocryst s.s. phases based on their abundances, appearance and chemistry (Fig. 8A, C). They are included in all portions of type 1 olivines and in the rims of the other olivine types (Fig. 10). The within-group chemical variation of these spinels (rapidly increasing TiO_2 and Fe^{3+} contents and restricted range of Cr#) reflects the effect of fractional crystallization of olivine that was the only phase co-precipitating with spinel (the studied clinopyroxenes contain titanomagnetites).

The cores of type 2a (Fig. 10B) and type 2b (Fig. 10C) olivines contain spinel inclusions of very different compositions: the former have group 1 spinels, while the latter have group 3 spinels (Fig. 8B–D). Such a strikingly large difference (more than 68 in their Cr#s) that is observed between the compositions of group 1 and group 3 spinels is inconsistent with crystallization from the same melt (e.g., Sack and Ghiorso, 1991). Since the composition of spinel depends primarily on the melt composition (e.g., Irvine, 1965, 1967; Dick and Bullen, 1984; Allan et al., 1988; Arai, 1992; Roeder, 1994; Kamenetsky et al., 2001), this significant difference in the Cr#s more likely reflects the group 1 and group 3 spinels having precipitated from two distinct melts characterised by different compositions. This means that the cores of type 2a olivines together with the group 1 spinels and the cores of type 2b olivines together with the group 3 spinels crystallised from two separate primitive magmas of dissimilar compositions. Thus, the cores of the type 2a and type 2b olivine crystals do not represent antecrysts of the same origin (antecryst 1a and antecryst 1b; Fig. 7).

	ol type	zoning	texture	features	sp incl.	interpretation
A	Type1	normal		euhedral-subhedral, skeletal, Fo decreases gradually rimward from 86 to 75 mol%	group2 sp in all portions	phenocryst *s.s.*; crystallization from M3
B	Type2a	normal		core: subhedral-anhedral, resorbed, 86-95 mol% Fo; rim: euhedral-subhedral, skeletal, 80-85 mol% Fo	group1 sp in the core, group2 sp in the rim	core: antecryst1a; rim: phenocryst *s.s.*; crystallization history: M1a → M3
C	Type2b	normal		core: subhedral-anhedral, resorbed, 86-91 mol% Fo; rim: euhedral-subhedral, skeletal, 80-85 mol% Fo	group3 sp in the core, group2 sp in the rim	core: antecryst1b; rim: phenocryst *s.s.*; crystallization history: M1b → M3
D	Type3	normal		core: anhedral, resorbed, 89-91 mol% Fo; rim: skeletal, 79-85 mol% Fo	group2 sp in the rim	core: xenocryst; rim: phenocryst *s.s.*; history: xenocryst incorporation → M3
E	Type4	reverse		core: subhedral-anhedral, resorbed, 66-85 mol% Fo; rim: euhedral-subhedral, skeletal, 76-86 mol% Fo	group2 sp in the rim	core: antecryst2; rim: phenocryst *s.s.*; crystallization history: M2 → M3
F	Type5	multiple		core: anhedral, resorbed, 89-90 mol% Fo; growth zone: subhedral, 83-85 mol% Fo; rim: skeletal, 82-86 mol% Fo	group2 sp in the rim	core: xenocryst; growth zone: antecryst2; rim: phenocryst *s.s.*; history: xenocryst incorporation → M2 → M3

Fig. 10. Summary of olivine textures, zoning and chemical characteristics (together with their spinel inclusions) as well as their interpretation concerning the formation of the different olivine types. M1a = magma 1a, M1b = magma 1b, M2 = magma 2, M3 = magma 3 which refer to the four magmatic environments.

In mafic and ultramafic volcanic rocks Cr-rich spinel (15–70 wt.% Cr_2O_3) is the most common spinel having compositions very similar to those of our group 2 and group 3 spinels. However, Al-rich spinels (Cr# < 5, Al_2O_3 > 50 wt.%) are rare in terrestrial volcanic rocks. Al-rich spinels similar to our group 1 spinels were rarely described from scarce continental mafic intrusions, lamproites, kimberlites and carbonatites (Barnes and Roeder, 2001) as well as from some primitive arc volcanics (Della-Pasqua et al., 1995). In the latter case, they also described coexisting Cr-rich and Al-rich spinels (as inclusions in olivines) which were inferred to have crystallised from melts of different compositions.

9.2. Magmatic environments and processes

The large variety of the olivine and spinel crystals, i.e., the liquidus phases indicates a complex magmatic system with four magmatic environments (Figs. 10 and 11) beneath the small-volume Kissomlyó volcano. The antecrystic cores of type 2a and type 2b olivines (i.e., antecryst 1a and antecryst 1b) derive from two primitive magmas (called magma 1a and magma 1b) characterised by different compositions based on the chemistry (group 1 and group 3) of their spinel inclusions. These primitive olivines and spinels probably represent the earliest stage of the evolution of the magmatic system. Differentiation of magma 1a through fractional crystallisation of antecryst 1a olivine together with group 1 spinel and that of magma 1b through fractional crystallisation of antecryst 1b olivine together with group 3 spinel could have taken place in the deepest part of the magmatic system. The majority of these early crystals were probably removed but a part of them were recycled by subsequent magma packets. On the basis of the studied olivines and spinels (Figs. 5–8) magma 1a could have been present in the system only during the second evolutionary phase, but magma 1b is inferred to have been involved during both evolutionary phases of the magmatic system.

The antecrystic cores of type 4 olivines (i.e., antecryst 2) could have been formed through magma differentiation in the shallower part of the system and are related to another magma, called magma 2. The reversely zoned feature of these olivines suggests magma recharge. As recorded by the compositions of their normally zoned rims the recharge magma is represented by the already differentiated magmas formed at deeper levels. This recharge magma recycled a number of more evolved olivine antecrysts and became dominant in the system. This dominant magma (representing the host magma) is called magma 3 from which type 1 olivines, the rims of each of the other olivine types and group 2 spinels crystallised followed by the formation of clinopyroxene phenocrysts as indicated by the textural relationships between olivines and clinopyroxenes.

Lithospheric mantle-derived olivine xenocrysts were incorporated by magma 2 and magma 3 recorded by type 5 and type 3 olivine crystals, respectively. This suggests that olivine crystallization from both magma 2 and magma 3 occurred in the lithospheric mantle.

The highly variable core compositions of the reversely zoned olivines and the recycling of different olivine antecrysts suggest that the evolution of the magmatic system could have been characterised by the involvement of multiple small magma. In addition, the variety of core compositions of reversely zoned olivines suggests that the mafic magmas could have been variably differentiated before a new more primitive magma intrusion arrived from depth. For simplicity, magma 1a, magma 1b, magma 2 and magma 3 refer to the four different magmatic environments (including the several small magma packets) where the distinct olivine and spinel populations crystallised.

In summary, the evolution of the magmatic system beneath Kissomlyó involved a complex set of petrogenetic processes: fractional crystallization, olivine (+ spinel) recycling, xenocryst incorporation, magma recharge and interaction of small magma packets, and each of these processes was operating during the whole life of the system. Through the stratigraphic succession, the juvenile basalt fragments of unit 1 contain the largest amount of reversely zoned olivines, i.e., the magma batch of the first eruption cycle brought the highest amount of antecryst 2 olivines to the surface. Based on this observation the formation of these more evolved olivine crystals could have been the most dominant during the first evolutionary phase, when magma packets
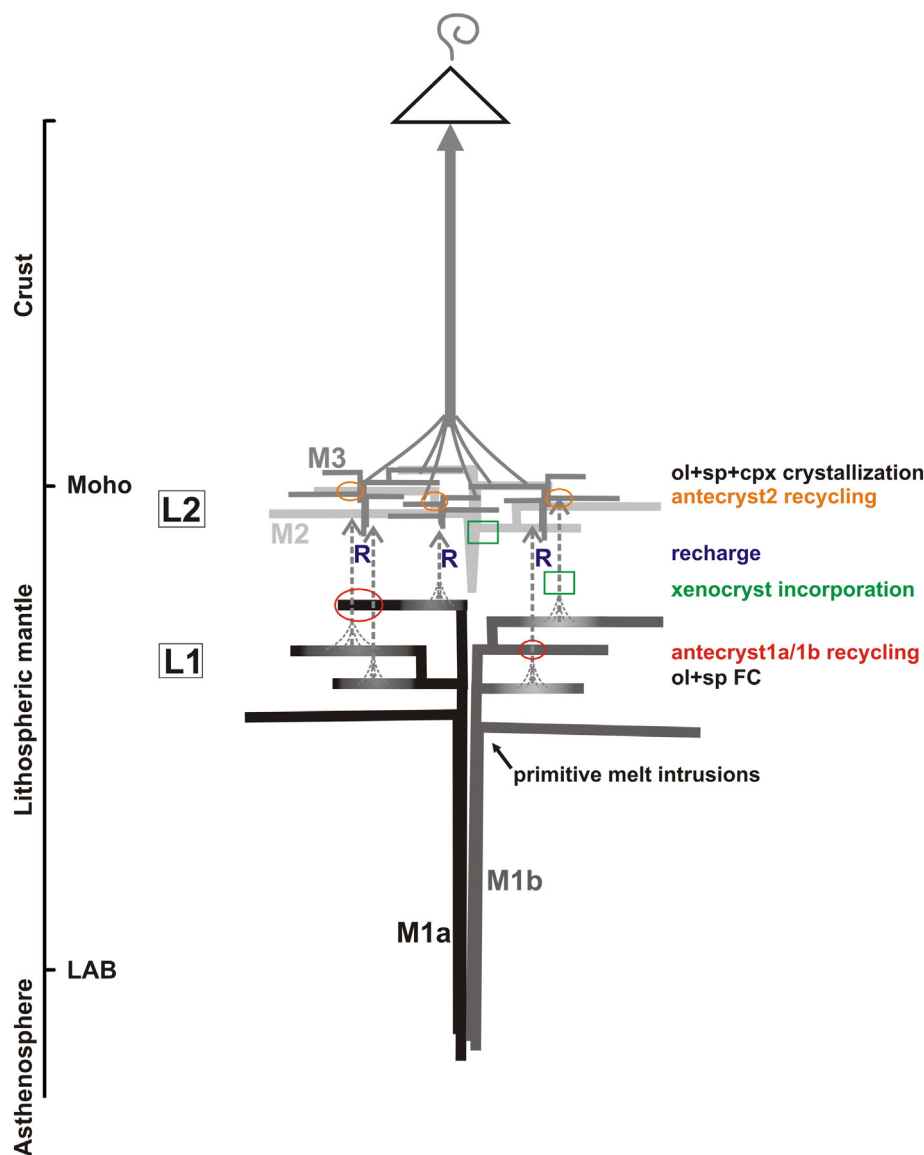
Fig. 11. Schematic model of the magmatic system beneath the Kissomlyó volcano (see text for discussion) with the petrogenetic processes of fractional crystallization, olivine ($+$spinel) recycling, xenocryst incorporation, magma recharge and interaction of small magma packets. The figure is not to scale. FC $=$ fractional crystallization, ol $=$ olivine, sp $=$ spinel, cpx $=$ clinopyroxene, LAB $=$ lithosphere-asthenosphere boundary. M1a $=$ magma 1a, M1b $=$ magma 1b, M2 $=$ magma 2, M3 $=$ magma 3 which refer to the four magmatic environments.

accumulated and trapped at a possible rheological/density boundary giving way to magma differentiation.

9.3. Multi-level magmatic system

On the basis of the revealed magmatic environments and deep-seated petrogenetic processes we propose a multi-level magmatic system beneath Kissomlyó (Fig. 11). It consists of two levels (level 1 and level 2) which are assumed being separated. At level 1 primitive magma intrusions occurred which went through olivine and spinel fractional crystallization resulting in the formation of fractionated melts. These melts ascended upwards, recycled primitive olivine antecrysts (antecrysts 1a and 1b) and recharged level 2 where they recycled antecryst 2 olivines from magma 2. This was followed by the in situ crystallization of olivine $+$ spinel and subsequent clinopyroxene (at level 2).

Based on experimental studies carried out on alkaline basalts, olivine crystallises as a liquidus phase (together with spinel) only at pressures ≤10 kbar (e.g., Green and Ringwood, 1967). This corresponds to depths

≤~37 km which means that level 1 of the system where early olivine $+$ spinel crystallised from primitive magmas was located at depths of maximum ~37 km, i.e., in the upper part of the lithospheric mantle, considering that the crustal thickness is around 26–27 km beneath the studied locality (Horváth, 1993).

Pressure values obtaining from clinopyroxene-melt barometry using clinopyroxene rim and coexisting glass compositions are generally interpreted as major levels of magma fractionation (e.g., Schwarz et al., 2004; Klügel et al., 2005; Galipp et al., 2006; Stroncik et al., 2009; Hildner et al., 2012). This method was used for numerous ocean island basalts (see the former references) and its good applicability was confirmed by the nice correlation of barometric results with geophysical data in the case of the recent El Hierro activity (Longpré et al., 2014).

The estimated pressure values reflect the conditions of last clinopyroxene-melt equilibration which is 6.6 $\pm$ 0.9 kbar average pressure in our case. This corresponds to a depth of about 25 km that can be placed just above the Moho (i.e., in the lowermost part of the crust). Since these data reflect the equilibrium conditions between

clinopyroxene rims and host melt (i.e., final clinopyroxene–melt equilibration), deeper fractionation for the clinopyroxene cores are possible (e.g., Hildner et al., 2012).

The textural relationships between olivine and clinopyroxene crystals indicate that the crystallization of olivines usually preceded that of clinopyroxenes. This can suggest that each type of olivines could have been formed at greater depths than clinopyroxenes, i.e., around and below the crust–mantle boundary. As level 1 is placed to a maximum depth of ~37 km, the lower boundary of the magmatic system is expected to be at depths ≤~37 km, while its upper boundary (the upper part of level 2) is given by the ~25 km depth indicated by the final clinopyroxene–melt equilibration. The exact extent of level 1 and level 2 cannot be determined.

A similar model of a multi-stage system consisting of a deeper and a shallower reservoir was presented in the case of the 2011–2012 El Hierro submarine activity on the strong basis of petrological, thermobarometric and seismic data (Martí et al., 2013; Longpré et al., 2014). They also described several types of olivines characterised by different zoning patterns, which were also inferred to bear evidence of open-system processes like magma replenishment and mixing.

9.4. What represents the whole-rock composition?

The whole-rock geochemical data of the three studied eruptive units (Fig. 3) do not show any abrupt, significant differences, thus the erupted magmas were compositionally similar during the entire volcanic activity. Although the compositional variation of the whole-rock data (Fig. 3C–F) do not indicate any complexities and could be explained by fractional crystallization of olivine + spinel, the high-resolution investigation of mineral textures, zoning and chemistry unravelled the complex evolution of the deep magmatic system. The erupted magma compositions represented by the bulk rock geochemistry are the results of various, closed- and open-system petrogenetic processes and interaction of multiple small magma packets in a multi-level system. The observed small differences between the whole-rock geochemistry of unit 1 and unit 2–unit 3 are most likely due to the variation in the proportions of the petrogenetic processes acting in the system during the two evolutionary phases.

Distinct eruptive units observed through basaltic monogenetic sequences are generally interpreted as representing discrete magma batches of different characteristics on the basis of their whole-rock geochemistry (e.g., Brenna et al., 2010; Mcgee et al., 2012; Sohn et al., 2012). These magma batches were also inferred to have interacted/mixed with each other based on the presence of units having whole-rock compositions transitional between those of the discrete magma batches. Brenna et al. (2012) described a bimodal distribution of olivine Fo contents and a wide whole-rock variation at Songaksan volcano (Jeju Island Volcanic Field). Based on these observations they proposed a model of mixing of ascending magma pulses (in a main plumbing conduit) which evolved in independent dykes before. However, in order to recognise the exact relationship between these magmas and to reveal the processes occurring during their ascent a detailed investigation of the olivine textures, zoning and chemistry would be necessary. It is important to note that through the analyses of whole-rock samples only the features of the erupted magma batches can be recognised, however, through the detailed mineral-scale investigations we can reveal the exact formation of these erupted magma batches, i.e., what kind of magmas (magma packets) were involved in the magmatic system and through which processes have they undergone ultimately resulting in a given erupted magma batch.

Our study indicates that the observed three eruptive units of Kissomlyó represent distinct magma batches having similar compositions but each magma erupted to the surface in the two main eruptive phases (represented by unit 1 and unit 2 + unit 3) is composed of several small magma packets which have interacted with each other in both evolutionary phases.

Whilst the whole-rock geochemical data show a relatively small variation (60.4–65.7 Mg#), the Fo contents of the cores of the magmatic (i.e., of type 1, type 2a + type 2b and type 4) olivines have a much broader range of compositions (Fo_{66-91}) indicating equilibrium liquid Mg#s ranging from 36 to 74 (Fig. 12). This large variation is due to the involvement of the four magmatic environments (magma 1a + magma 1b, magma 2 and magma 3) crystallising the different olivine (and spinel) populations. The very Fo-rich olivine clot (Fig. 6B) was excluded from the equilibrium liquid Mg# calculation because of its too high Fo content that may suggest a non-equilibrium/non-ideal/different $K_D(Fe-Mg)$ in this case. However, their enclosed spinel inclusions indicate that they have magmatic origin and belong to the antecryst 1a population.

9.5. Comparison with other monogenetic sequences

Fig. 4 shows a comparison with other monogenetic eruptive centres: the Crater Hill (Smith et al., 2008) and Motukorea (Mcgee et al., 2012) in
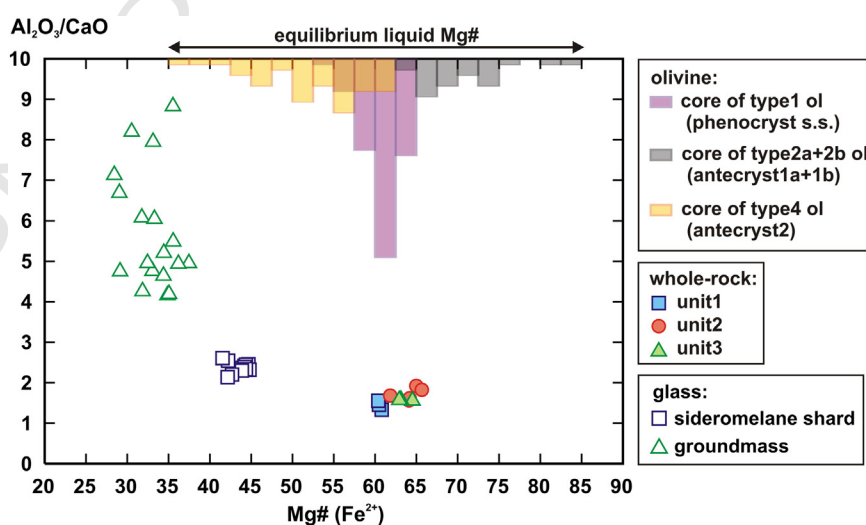
Fig. 12. Mg# (Mg/(Mg + Fe^{2+})) vs. Al$_2$O$_3$/CaO plot that shows the whole-rock data from the three eruptive units, the glass compositions of the sideromelane glass shards (unit 1) and groundmass glass (unit 3) as well as a histogram showing the equilibrium liquid Mg#s calculated for the cores of type 1, type 2a + type 2b and type 4 olivines (transitional colours are due to overlapping columns). Note the broad compositional range indicated by these magmatic olivines compared to the small Mg# variation of the whole-rock and glass compositions.

the Auckland Volcanic Field, the Udo volcano (Brenna et al., 2010), the Songaksan volcanic centre (Brenna et al., 2011) and the Ilchulbong tuff cone (Sohn et al., 2012), all of the latter three located in the Jeju Island Volcanic Field. Additionally, we included the case of the 2011–2012 El Hierro activity, Canary Islands (analysed samples: from 15 October 2011 to 28 January 2012; Martí et al., 2013) that also represents a monogenetic event. In the case of these eruptive centres the presented geochemical datasets are the results of a higher-resolution sampling. This can be explained by the presence of several discontinuity surfaces/event horizons through their sequences (resulted in the recognition of several subunits) and by the larger volumes of these volcanics comparing to those of Kissomlyó. Nevertheless, our dataset is comparable with these because our sampling was appropriate for the given scale. The detailed studies on the mentioned volcanic centres do not infer significant time gap(s) during their volcanic activities, i.e., their evolution reflect a short period of time (within days to months). However, significant compositional variations were observed through time/successions between and/or within the individual eruptive units. Although most of them show fluctuations in their compositional evolutions, their trends have a significant reverse part moving towards more primitive compositions through time/the units upward in the sequence. These compositional variations suggest that monogenetic eruptive centres are fed by dynamically changing magmatic systems. It is notable, that in the case of the Kissomlyó volcano, where a considerable time gap is assumed in the volcanic activity (recorded by the lacustrine sediments between the tuff ring pyroclastics and the lava flow) the observable chemical variation is smaller than those of the others.

In the evolution of a magmatic system the volume of the involved magmas can have an important role: in the case of low-volume magmas they cool and quench rapidly which do not enable significant magmatic differentiation. The Kissomlyó volcanic centre can be characterised by a small total eruptive volume (~0.002 km^3) and if we consider separately the volumes of the individual eruptive units (~0.001 km^3) it would be expected that the magma supply could have been very low. However, the eruptive volume seen on the surface does not represent the real volume of magmas being involved in the evolution of the deep magmatic system beneath the volcanoes. Therefore, the magma productivity can be significantly larger than what is indicated by the total eruptive volume. This could be feasible in the case of the Kissomlyó volcanic centre where the whole-rock compositions as well as the presence of abundant clinopyroxene phenocrysts and more evolved olivine antecrysts indicate fairly considerable magmatic differentiation.

The relationship between the sizes and compositions of eruptive centres was studied in the case of the Auckland Volcanic Field, New Zealand by Mcgee et al. (2013) who found strong correlations and concluded that the size of a volcanic centre is controlled by processes in the deep asthenosphere. However, they have not discussed the relationship between the size (eruptive volume) of volcanic centres and their intra-centre compositional variations. Based on their presented dataset the compositional variations within the eruptive centres do not depend on the eruptive volumes: a small centre can be characterised by the same significant chemical variation that is observed in the case of a large centre and also a large centre can have a compositional variation smaller than that of a small centre. Volcanic centres showing a small intra-centre chemical variation similar to that of Kissomlyó are rare. Additionally, the centre having very similar small eruptive volume shows much larger intra-centre compositional variation than Kissomlyó.

All of these imply that although the Kissomlyó volcano has a very small eruptive volume and a small intra-centre whole-rock chemical variation its deep magmatic system was characterised by a complex evolution history.

10. Conclusions

The evolution of the magmatic system beneath the small-volume Kissomlyó monogenetic volcano was inferred as being complex documented by mineral textures, zoning and chemistry. Five different types of olivine crystals and three distinct compositional groups of olivine-hosted spinel inclusions were recognised which represent four magmatic environments. These crystals bear evidence of several petrogenetic processes that played role in the formation of the erupted magma batches: fractional crystallization, olivine (+ spinel) recycling, lithospheric mantle-derived xenocryst incorporation, magma recharge and interaction of multiple small magma packets.

Reversely zoned olivines suggest the presence of evolved magmas, while high-Fo olivine cores imply primitive magmas at depth which did not erupt to the surface but are detectable by the olivine antecrysts found in the host magma.

Barometric results of final clinopyroxene–melt equilibration indicate that clinopyroxene crystallization could have occurred around the Moho, which was preceded by the formation of the diverse olivine crystals.

Our study implies that the petrogenesis of a single magma batch (usually defined as representing a given eruptive unit) can be complex involving several magmas and various, closed- and open-system magmatic processes which finally result in the whole-rock (erupted magma) composition.

Beyond the bulk rock geochemistry, the high-resolution investigation of the textures, zoning and chemistry of minerals through the sequence of monogenetic volcanoes provides a more detailed insight into the deep magmatic processes and into the characteristics of the magmas being involved in the evolution of the magmatic system. Such a detailed mineral-scale analysis is a very useful tool that yields a lot of important knowledge about the magmatic system which are essential to our better understanding about the evolution of "simple" basaltic monogenetic systems.

11. Uncited reference   Q6

Valentine and Perry, 2007

References

Ali, S., Ntaflos, T., 2011. Alkali basalts from Burgenland, Austria: petrological constraints on the origin of the westernmost magmatism in the Carpathian-Pannonian Region. Lithos 121 (1-4), 176–188.

Allan, J.F., Sack, R.O., Batiza, R., 1988. Cr-rich spinels as petrogenetic indicators; MORB-type lavas from the Lamont seamount chain, eastern Pacific. Am. Mineral. 73 (7-8), 741–753.

Arai, S., 1992. Chemistry of chromian spinel in volcanic rocks as a potential guide to magma chemistry. Mineral. Mag. 56, 173–184.

Auer, A., Martin, U., Németh, K., 2007. The Fekete-hegy (Balaton Highland Hungary) "soft-substrate" and "hard-substrate" maar volcanoes in an aligned volcanic complex – Implications for vent geometry, subsurface stratigraphy and the palaeoenvironmental setting. J. Volcanol. Geotherm. Res. 159 (1–3), 225–245.

Bada, G., Horváth, F., 2001. On the structure and tectonic of the Pannonian Basin and surrounding orogens. Acta Geol. Hung. 44 (2-3), 301–327.

Balogh, K., Árva-Sós, E., Pécskay, Z., Ravasz-Baranyai, L., 1986. K/Ar dating of post-Sarmatian alkali basaltic rocks in Hungary. Acta Mineral. Petrogr. Szeged. 28, 75–93.

Barnes, S.J., Roeder, P.L., 2001. The range of spinel compositions in terrestrial mafic and ultramafic rocks. J. Petrol. 42 (12), 2279–2302.

Boudier, F., 1991. Olivine xenocrysts in picritic magmas: an experimental and microstructural study. Contrib. Mineral. Petrol. 109 (1), 114–123.

Boyce, J., Nicholls, I., Keays, R., Hayman, P., 2015. Variation in parental magmas of Mt Rouse, a complex polymagmatic monogenetic volcano in the basaltic intraplate Newer Volcanics Province, southeast Australia. Contrib. Mineral. Petrol. 169 (2), 1–21.

Brenna, M., Cronin, S.J., Smith, I.E.M., Sohn, Y.K., Németh, K., 2010. Mechanisms driving polymagmatic activity at a monogenetic volcano, Udo, Jeju Island, South Korea. Contrib. Mineral. Petrol. 160 (6), 931–950.

Brenna, M., Cronin, S.J., Németh, K., Smith, I.E.M., Sohn, Y.K., 2011. The Influence of Magma Plumbing Complexity on Monogenetic Eruptions, Jeju Island, Korea. Terra Nova. pp. 1–6.

Brenna, M., Cronin, S.J., Smith, I.E.M., Maas, R., Sohn, Y.K., 2012. How small-volume basaltic magmatic systems develop: a case study from the Jeju Island Volcanic Field, Korea. J. Petrol. 53 (5), 985–1018.

Connor, C.B., Conway, F.M., 2000. Basaltic Volcanic Fields. In: Sigurdsson, H. (Ed.), Encyclopedia of Volcanoes. Academic Press, San Diego, pp. 331–343.

Csontos, L., Nagymarosy, A., Horváth, F., Kovác, M., 1992. Tertiary evolution of the Intra-Carpathian area: a model. Tectonophysics 208 (1-3), 221–241.

Della-Pasqua, F.N., Kamenetsky, V.S., Gasparon, M., Crawford, A.J., Varne, R., 1995. Al-spinels in primitive arc volcanics. Mineral. Petrol. 53 (1-3), 1–26.

Dick, H.J.B., Bullen, T., 1984. Chromian spinel as a petrogenetic indicator in abyssal and alpine-type peridotites and spatially associated lavas. Contrib. Mineral. Petrol. 86 (1), 54–76.

Dobosi, G., 1989. Clinopyroxene zoning patterns in the young alkali basalts of Hungary and their petrogenetic significance. Contrib. Mineral. Petrol. 101, 112–121.

Dobosi, G., Schultz-Güttler, R., Kurat, G., Kracher, A., 1991. Pyroxene chemistry and evolution of alkali basaltic rocks from Burgenland and Styria, Austria. Mineral. Petrol. 43 (4), 275–292.

Embey-Isztin, A., Downes, H., James, D.E., Upton, B.G.J., Dobosi, G., Ingram, G.A., Harmon, R.S., Scharbert, H.G., 1993. The petrogenesis of Pliocene alkaline volcanic rocks from the Pannonian Basin, Eastern Central Europe. J. Petrol. 34, 317–343.

Embey-Isztin, A., Dobosi, G., Altherr, R., Meyer, H.-P., 2001. Thermal evolution of the lithosphere beneath the western Pannonian Basin: evidence from deep-seated xenoliths. Tectonophysics 331 (3), 285–306.

Erlund, E.J., Cashman, K.V., Wallace, P.J., Pioli, L., Rosi, M., Johnson, E., Granados, H.D., 2010. Compositional evolution of magma from Parícutin Volcano, Mexico: the tephra record. J. Volcanol. Geotherm. Res. 197 (1–4), 167–187.

Fodor, L., Csontos, L., Bada, G., Benkovics, L., Györfi, I., 1999. Tertiary tectonic evolution of the Carpatho-Pannonian region: a new synthesis of palaeostress data. In: Durand, B., Jolivet, L.F.H., Séranne, M. (Eds.), The Mediterranean basins: tertiary extension within the Alpine Orogen. Geological Society, London, Special Publications 156, pp. 295–334.

Galipp, K., Klügel, A., Hansteen, T.H., 2006. Changing depths of magma fractionation and stagnation during the evolution of an oceanic island volcano: La Palma (Canary Islands). J. Volcanol. Geotherm. Res. 155 (3–4), 285–306.

Ginibre, C., Wörner, G., Kronz, A., 2007. Crystal zoning as an archive for magma evolution. Elements 3 (4), 261–266.

Granet, M., Wilson, M., Achauer, U., 1995. Imaging a mantle plume beneath the French Massif Central. Earth Planet. Sci. Lett. 136 (3-4), 281–296.

Green, D.H., Ringwood, A.E., 1967. The genesis of basaltic magmas. Contrib. Mineral. Petrol. 15 (2), 103–190.

Harangi, S., 2001a. Neogene to quaternary volcanism of the Carpathian–Pannonian region—a review. Acta Geol. Hung. 44, 223–258.

Harangi, S., 2001b. Neogene magmatism in the Alpine–Pannonian Transition Zone—a model for melt generation in a complex geodynamic setting. Acta Vulcanol. 13, 25–39.

Harangi, S., 2001c. Volcanology and petrology of the Late Miocene to Pliocene alkali basaltic volcanism in the Western Pannonian Basin. In: Ádám, A., Szarka, L. (Eds.), PANCARDI 2001 Field Guide, Sopron, pp. 51–81.

Harangi, S., 2009. Volcanism of the Carpathian-Pannonian region, Europe: the role of subduction, extension and mantle plumes. http://www.mantleplumes.org/CarpathianPannonian.html.

Harangi, S., Lenkey, L., 2007. Genesis of the Neogene to Quaternary volcanism in the Carpathian–Pannonian region: role of subduction, extension, and mantle plume. Geol. Soc. Am. Spec. Pap. 418, 67–92.

Harangi, S., Vaseili, O., Kovács, R., Tonarini, S., Coradossi, N., Ferraro, D., 1994. Volcanological and magmatological studies on the Neogene basaltic volcanoes of the Southern Little Hungarian Plain, Pannonian Basin (Western Hungary). Mineral. Petrogr. Acta 37, 183–197.

Harangi, S., Vaselli, O., Tonarini, S., Szabó, C., Harangi, R., Coradossi, N., 1995. Petrogenesis of Neogene extension-related alkaline volcanic rocks of the Little Hungarian Plain Volcanic Field (Western Hungary). Acta Vulcanol. 7 (2), 173–187.

Harangi, S., Sági, T., Seghedi, I., Ntaflos, T., 2013. Origin of basaltic magmas of Perşani volcanic field, Romania: a combined whole rock and mineral scale investigation. Lithos 180–181, 43–57.

Harangi, S., Jankovics, M.É., Sági, T., Kiss, B., Lukács, R., Soós, I., 2014. Origin and geodynamic relationships of the Late Miocene to Quaternary alkaline basalt volcanism in the Pannonian basin, eastern–central Europe. Int. J. Earth Sci. 1–26.

Hildner, E., Klügel, A., Hansteen, T.H., 2012. Barometry of lavas from the 1951 eruption of Fogo, Cape Verde Islands: implications for historic and prehistoric magma plumbing systems. J. Volcanol. Geotherm. Res. 217–218, 73–90.

Hirano, N., Yamamoto, J., Kagi, H., Ishii, T., 2004. Young, olivine xenocryst-bearing alkali-basalt from the oceanward slope of the Japan Trench. Contrib. Mineral. Petrol. 148 (1), 47–54.

Hoernle, K., Zhang, Y.S., Graham, D., 1995. Seismic and geochemical evidence for large-scale mantle upwelling beneath the eastern Atlantic and western and central Europe. Nature 374, 34–39.

Horváth, F., 1993. Towards a mechanical model for the formation of the Pannonian Basin. Tectonophysics 226 (1-4), 333–357.

Horváth, F., 1995. Phases of compression during the evolution of the Pannonian Basin and its bearing on hydrocarbon exploration. Mar. Pet. Geol. 12 (8), 837–844.

Horváth, F., Cloetingh, S., 1996. Stress-induced late-stage subsidence anomalies in the Pannonian Basin. Tectonophysics 266 (1-4), 287–300.

Irvine, T.N., 1965. Chromian spinel as a petrogenetic indicator: Part 1. Theory. Can. J. Earth Sci. 2 (6), 648–672.

Irvine, T.N., 1967. Chromian spinel as a petrogenetic indicator: Part 2. Petrologic applications. Can. J. Earth Sci. 4 (1), 71–103.

Jankovics, É., Harangi, S., Ntaflos, T., 2009. A mineral-scale investigation on the origin of the 2.6 Ma Füzes-tó basalt, Bakony-Balaton Highland Volcanic Field (Pannonian Basin, Hungary). Cen. Eur. Geol. 52 (2), 97–124.

Jankovics, M.É., Harangi, S., Kiss, B., Ntaflos, T., 2012. Open-system evolution of the Füzes-tó alkaline basaltic magma, western Pannonian Basin: constraints from mineral textures and compositions. Lithos 140–141, 25–37.

Jankovics, M.É., Dobosi, G., Embey-Isztin, A., Kiss, B., Sági, T., Harangi, S., Ntaflos, T., 2013. Origin and ascent history of unusually crystal-rich alkaline basaltic magmas from the western Pannonian Basin. Bull. Volcanol. 75 (9), 1–23.

Jugovics, L., 1915. Az Alpok keleti végződése alján és a Vas vármegyei Kis Magyar Alföldön felbukkanó bazaltok és bazalttufák, I. rész (in Hungarian). Magyar Állami Földtani Intézet Évi Jelentésepp. 49–73.

Jugovics, L., 1916. Az Alpok keleti végződése alján és a Vas vármegyei Kis Magyar Alföldön felbukkanó bazaltok és bazalttufák, II. rész (in Hungarian). Magyar Állami Földtani Intézet Évi Jelentésepp. 63–76.

Jugovics, L., 1968. A dunántúli bazalt és bazalttufa területek (in Hungarian). A Magyar Állami Földtani Intézet Évi Jelentése az 1967pp. 75–82 évről.

Kahl, M., Chakraborty, S., Costa, F., Pompilio, M., 2011. Dynamic plumbing system beneath volcanoes revealed by kinetic modeling, and the connection to monitoring data: an example from Mt. Etna. Earth Planet. Sci. Lett. 308 (1–2), 11–22.

Kamenetsky, V.S., Crawford, A.J., Meffre, S., 2001. Factors controlling chemistry of magmatic spinel: an empirical study of associated olivine, Cr-spinel and melt inclusions from primitive rocks. J. Petrol. 42 (4), 655–671.

Kereszturi, G., Csillag, G., Németh, K., Sebe, K., Balogh, K., Jáger, V., 2010. Volcanic architecture, eruption mechanism and landform evolution of a Plio/Pleistocene intracontinental basaltic polycyclic monogenetic volcano from the Bakony-Balaton Highland Volcanic Field, Hungary. Cent. Eur. J. Geosci. 2 (3), 362–384.

Kereszturi, G., Németh, K., Cronin, S.J., Agustín-Flores, J., Smith, I.E.M., Lindsay, J., 2013. A model for calculating eruptive volumes for monogenetic volcanoes — Implication for the Quaternary Auckland Volcanic Field, New Zealand. J. Volcanol. Geotherm. Res. 266, 16–33.

Klügel, A., Hansteen, T.H., Galipp, K., 2005. Magma storage and underplating beneath Cumbre Vieja volcano, La Palma (Canary Islands). Earth Planet. Sci. Lett. 236 (1–2), 211–226.

Konečný, V., Lexa, J., Balogh, K., Konečný, P., 1995. Alkali basalt volcanism in Southern Slovakia: volcanic forms and time evolution. Acta Vulcanol. 7 (2), 167–171.

Lenkey, L., Dövényi, P., Horváth, F., Cloetingh, S., 2002. Geothermics of the Pannonian Basin and its bearing on the neotectonics. European Geophysical Union Stephan Mueller Special Publications, Series 3 pp. 29–40.

Longpré, M.-A., Klügel, A., Diehl, A., Stix, J., 2014. Mixing in mantle magma reservoirs prior to and during the 2011–2012 eruption at El Hierro, Canary Islands. Geology 42 (4), 315–318.

Martí, J., Castro, A., Rodríguez, C., Costa, F., Carrasquilla, S., Pedreira, R., Bolos, X., 2013. Correlation of magma evolution and geophysical monitoring during the 2011–2012 El Hierro (Canary Islands) Submarine Eruption. J. Petrol. 54 (7), 1349–1373.

Martin, U., Németh, K., 2004. Mio/Pliocene Phreatomagmatic Volcanism in the Western Pannonian Basin. Geological Institute of Hungary, Budapest.

Martin, U., Németh, K., 2005. Eruptive and depositional history of a Pliocene tuff ring that developed in a fluvio-lacustrine basin: Kissomlyó volcano (western Hungary). J. Volcanol. Geotherm. Res. 147 (3-4), 342–356.

Mcgee, L., Beier, C., Smith, I.M., Turner, S., 2011. Dynamics of melting beneath a small-scale basaltic system: a U–Th–Ra study from Rangitoto volcano, Auckland volcanic field, New Zealand. Contrib. Mineral. Petrol. 162 (3), 547–563.

Mcgee, L.E., Millet, M.-A., Smith, I.E.M., Németh, K., Lindsay, J.M., 2012. The inception and progression of melting in a monogenetic eruption: Motukorea Volcano, the Auckland Volcanic Field, New Zealand. Lithos 155, 360–374.

Mcgee, L.E., Smith, I.E.M., Millet, M.-A., Handley, H.K., Lindsay, J.M., 2013. Asthenospheric control of melting processes in a monogenetic basaltic system: a case study of the Auckland Volcanic Field, New Zealand. J. Petrol. 54 (10), 2125–2153.

Morimoto, N., Fabries, J., Ferguson, A.K., Ginzburg, I.V., Ross, M., Seifert, F.A., Zussman, J., Aoki, K., Gottardi, G., 1988. Nomenclature of pyroxenes. Mineral. Mag. 52, 535–550.

Nakamura, N., 1974. Determination of REE, Ba, Fe, Mg, Na and K in carbonaceous and ordinary chondrites. Geochim. Cosmochim. Acta 38 (5), 757–775.

Needham, A.J., Lindsay, J.M., Smith, I.E.M., Augustinus, P., Shane, P.A., 2011. Sequential eruption of alkaline and sub-alkaline magmas from a small monogenetic volcano in the Auckland Volcanic Field, New Zealand. J. Volcanol. Geotherm. Res. 201 (1–4), 126–142.

Németh, K., 2010. Monogenetic volcanic fields: origin, sedimentary record, and relationship with polygenetic volcanism. Geol. Soc. Am. Spec. Pap. 470, 43–66.

Németh, K., Martin, U., Harangi, S., 2001. Miocene phreatomagmatic volcanism at Tihany (Pannonian Basin, Hungary). J. Volcanol. Geotherm. Res. 111 (1–4), 111–135.

Németh, K., Moufti, M.R., El-Masry, N., Qaddah, A., Pécskay, Z., 2014. Maars over cones: repeated volcanism in the same location along fissures in western Saudi Arabian volcanic fields. In: Carrasco-Núñez, G., Aranda-Gómez, J.J., Ort, M.H., Silva-Corona, J.J. (Eds.), 5th International Maar Conference. Universidad Nacional Autónoma de México, Centro de Geociencias, Juriquilla, Qro., México, pp. 2–3.

Putirka, K., 1999. Clinopyroxene + liquid equilibria to 100 kbar and 2450 K. Contrib. Mineral. Petrol. 135 (2-3), 151–163.

Putirka, K.D., 2008. Thermometers and barometers for volcanic systems. Rev. Mineral. Geochem. 69 (1), 61–120.

Putirka, K.D., Mikaelian, H., Ryerson, F., Shaw, H., 2003. New clinopyroxene–liquid thermobarometers for mafic, evolved, and volatile-bearing lava compositions, with applications to lavas from Tibet and the Snake River Plain, Idaho. Am. Mineral. 88 (10), 1542–1554.

Reubi, O., Nicholls, I.A., Kamenetsky, V.S., 2003. Early mixing and mingling in the evolution of basaltic magmas: evidence from phenocryst assemblages, Slamet Volcano, Java, Indonesia. J. Volcanol. Geotherm. Res. 119 (1–4), 255–274.

Roeder, P.L., 1994. Chromite: from the fiery rain of chondrules to the Kilauea Iki lava lake. Can. Mineral. 32 (4), 729–746.

Roeder, P.L., Emslie, R.F., 1970. Olivine-liquid equilibrium. Contrib. Mineral. Petrol. 29 (4), 275–289.

Roeder, P.L., Poustovetov, A., Oskarsson, N., 2001. Growth forms and composition of chromian spinel in MORB magma: diffusion-controlled crystallization of chromian spinel. Can. Mineral. 39 (2), 397–416.

Roeder, P.L., Thornber, C., Poustovetov, A., Grant, A., 2003. Morphology and composition of spinel in Pu'u 'O'o lava (1996–1998), Kilauea volcano, Hawaii. J. Volcanol. Geotherm. Res. 123 (3-4), 245–265.

Roeder, P., Gofton, E., Thornber, C., 2006. Cotectic Proportions of Olivine and Spinel in Olivine-Tholeiitic Basalt and Evaluation of Pre-Eruptive Processes. J. Petrol. 47 (5), 883–900.

Sack, R.O., Ghiorso, M.S., 1991. Chromian spinels as petrogenetic indicators; thermodynamics and petrological applications. Am. Mineral. 76 (5-6), 827–847.

Schwarz, S., Klügel, A., Wohlgemuth-Ueberwasser, C., 2004. Melt extraction pathways and stagnation depths beneath the Madeira and Desertas rift zones (NE Atlantic) inferred from barometric studies. Contrib. Mineral. Petrol. 147 (2), 228–240.

Seghedi, I., Downes, H., Vaselli, O., Szakács, A., Balogh, K., Pécskay, Z., 2004. Post-collisional Tertiary–Quaternary mafic alkalic magmatism in the Carpathian-Pannonian region: a review. Tectonophysics 393 (1-4), 43–62.

Shane, P., Gehrels, M., Zawalna-Geer, A., Augustinus, P., Lindsay, J., Chaillou, I., 2013. Longevity of a small shield volcano revealed by crypto-tephra studies (Rangitoto volcano, New Zealand): change in eruptive behavior of a basaltic field. J. Volcanol. Geotherm. Res. 257, 174–183.

Smith, D.R., Leeman, W.P., 2005. Chromian spinel-olivine phase chemistry and the origin of primitive basalts of the southern Washington Cascades. J. Volcanol. Geotherm. Res. 140 (1-3), 49–66.

Smith, I.E.M., Blake, S., Wilson, C.J.N., Houghton, B.F., 2008. Deep-seated fractionation during the rise of a small-volume basalt magma batch: Crater Hill, Auckland, New Zealand. Contrib. Mineral. Petrol. 155 (4), 511–527.

Sohn, Y.K., Cronin, S.J., Brenna, M., Smith, I.E.M., Németh, K., White, J.D.L., Murtagh, R.M., Jeon, Y.M., Kwon, C.W., 2012. Ilchulbong tuff cone, Jeju Island, Korea, revisited: a compound monogenetic volcano involving multiple magma pulses, shifting vents, and discrete eruptive phases. Geol. Soc. Am. Bull. 124 (3-4), 259–274.

Streck, M.J., 2008. Mineral textures and zoning as evidence for open system processes. Rev. Mineral. Geochem. 69 (1), 595–622.

Stroncik, N., Klügel, A., Hansteen, T., 2009. The magmatic plumbing system beneath El Hierro (Canary Islands): constraints from phenocrysts and naturally quenched basaltic glasses in submarine rocks. Contrib. Mineral. Petrol. 157 (5), 593–607.

Strong, M., Wolff, J., 2003. Compositional variations within scoria cones. Geology 31 (2), 143–146.

Suhr, P., Goth, K., 2013. The Maar of Hammerunterwiesenthal—a "Complex Monogenetic Volcano", Saxony. In: Büchner, J., Rapprich, V., Tietz, O. (Eds.), Basalt 2013 Cenozoic Magmatism in Central Europe. Czech Geological Survey Prague & Senckenberg Museum of Natural History Görlitz, Görlitz, Germany, pp. 145–146.

Takada, A., 1994. The influence of regional stress and magmatic input on styles of monogenetic and polygenetic volcanism. J. Geophys. Res. 99 (B7), 13563–13573.

Tari, G., Horváth, F., Rumpler, J., 1992. Styles of extension in the Pannonian Basin. Tectonophysics 208 (1–3), 203–219.

Tari, G., Dövényi, P., Horváth, F., Dunkl, I., Lenkey, L., Stefanescu, M., Szafián, P., Tóth, T., 1999. Lithospheric structure of the Pannonian Basin derived from seismic, gravity and geothermal data. In: Durand, B., Jolivet, L., Horváth, F., Séranne, M. (Eds.), The Mediterranean basins: tertiary extension within the Alpine orogen. Geological Society, London, Special Publication 156, pp. 215–250.

Tracy, R.J., Robinson, P., 1977. Zoned titanian augite in alkali olivine basalt from Tahiti and the nature of titanium substitutions in augite. Am. Mineral. 62 (7-8), 634–645.

Valentine, G.A., Perry, F.V., 2007. Tectonically controlled, time-predictable basaltic volcanism from a lithospheric mantle source (central Basin and Range Province, USA). Earth Planet. Sci. Lett. 261 (1–2), 201–216.

Wass, S.Y., 1973. The origin and petrogenetic significance of hour-glass zoning in titaniferous clinopyroxenes. Mineral. Mag. 39 (302), 133–144.

Wijbrans, J., Németh, K., Martin, U., Balogh, K., 2007. 40Ar/39Ar geochronology of Neogene phreatomagmatic volcanism in the western Pannonian Basin, Hungary. J. Volcanol. Geotherm. Res. 164 (4), 193–204.